

THESIS

APPLICATION OF GROUND PENETRATING RADAR TO SUB-ALPINE
HYDROGEOLOGY, SNOWY RANGE, WYOMING.

Submitted by

Nathan Page

Department of Geosciences

In partial fulfillment of the requirements

For the Degree of Master of Science

Colorado State University

Fort Collins, Colorado

Summer 2011

Master's Committee:

Advisor: Dennis Harry

Co-Advisor: John Stednick

Gregory Butters

Michael Ronayne

ABSTRACT

APPLICATION OF GROUND PENETRATING RADAR TO SUB-ALPINE HYDROGEOLOGY, SNOWY RANGE, WYOMING.

A ground penetrating radar (GPR) survey was conducted at the Glacier Lakes Ecosystem Experiment Site, in the Snowy Range of Wyoming with the objective of determining the potential groundwater storage in the sediment overburden and determining the bedrock fracture density. The survey was completed along 12 transects with 100 MHz antennas using a Sensors and Software[®] PulseEKKO[®] 100 system. The step size between shots was 0.25 meters and the separation between the antennas was 1 meter. Two common midpoint (CMP) surveys were conducted and the subsurface GPR velocity was determined to be 0.06 m/ns.

The survey results indicate that sediment overburden thickness ranges from 0 m at bedrock outcrops to > 9 m near East Glacier Lake. The volume of sediment at the study site estimated at $83,800 \pm 8,380 \text{ m}^3$. Based on a grainsize analysis of representative soil pedons the average specific yield at the study site is estimated to be approximately 10%. Given these values for soil volume and specific yield, the potential groundwater storage is $8,380 \pm 838 \text{ m}^3$ for the study site, which extrapolates to $61,300 \pm 6,130 \text{ m}^3$ in groundwater storage in the East Glacier Lake watershed. The two dimensional bedrock

fracture density was determined to be 1 fracture per 4,810 m². The bedrock groundwater storage is undetermined.

TABLE OF CONTENTS

1.	Introduction.....	1
2.	Description of GLEES	3
3.	Previous Work	7
4.	Methods.....	9
4.1	Theory	9
4.2	Field Protocol.....	14
4.3	Radar Facies.....	21
4.4	Creating an Isochore Map.....	22
4.5	Estimating Maximum Storage and $Q_{gw,out}$	23
5.	Results.....	24
6.	Uncertainty.....	37
7.	Discussion.....	40
8.	Conclusions.....	43
9.	Recommendations for Future Study	44
10.	References.....	46
	Appendix A: GPR Transects.....	49

LIST OF TABLES

Table 1. - Common values for relative dielectric permittivity, electromagnetic wave velocity, conductivity and attenuation in associated geologic mediums (modified from Neal, 2004).....	12
Table 2. - Typical values of reflection coefficients for some common subsurface geologic interfaces. Values range from +1 to -1, the sign indicating polarity of the reflected wave (modified from Neal, 2004).....	13

LIST OF FIGURES

Figure 1. - Geographical location of GLEES.....	1
Figure 2. - Regional map of GLEES. Outline of GLEES from Musselman et al. (1992). Digital elevation model obtained from the Wyoming Geographic Information Science Center (http://www.uwyo.edu/wygisc).....	2
Figure 3. - Soil type map of study area (modified from Hopper and Walthall, 1992).	7
Figure 4. - a) Common offset survey mode: transmitting antenna (T) and receiving antenna (R) are held at a constant offset and stepped sequentially along the survey transect after each shot b) Common midpoint (CMP) survey mode: T and R are equally offset at greater distances apart following each shot. The midpoint between the two antennas remains constant and therefore remains the target of acquisition throughout the survey.....	15
Figure 5. - Topographic study site map showing survey transect layout, bedrock outcrop locations, CMP survey locations and the location of the East Glacier Lake outlet stream Parshall flume gauge. Elevations are reported relative to the water level of East Glacier Lake (3,282m amsl). Two areas of interest were surveyed; the median between East and West Glacier Lakes (transects L1, T1, T2 and T3) and the area of non-channelized inflow and the outlet stream on the east side of East Glacier Lake (transects L2, L3, T4a, T4b, T5, T6, T7 and T8).....	16
Figure 6. - Graphical illustration of the GPR processing sequence used in this study.....	18
Figure 7. - a) Semblance analysis of the common midpoint (CMP) survey. The warmer colors indicate the most likely radar velocities. b) Example of comparison of hyperbolic fit to diffractions in the radar data. The average velocity determined from these analyses is 0.06m/ns. Note strong sublinear moveout feature dipping to right with an apparent velocity of 0.15 m/ns. This is a subsurface reflection.....	19
Figure 8. - The average amplitude spectrum plot for transect T2 before and after application of the temporal low-pass filter.	21
Figure 9. - Description and geologic interpretation of the radar facies used in the interpretation of the GPR dataset.....	22

Figure 10. - Isochore map of sediment overburden. The contour lines represent sediment thickness. The sediment is generally thicker in valleys and thinner on ridges. Notice the isolated deep pocket of sediment located on transect T1..... 25

Figure 11. - GPR transect T2. Elevation is relative to the water level of East Glacier Lake (3,282m amsl). Depths below ground level are based on an average radar velocity of 0.06 m/ns. 26

Figure 12. - a) Interpreted GPR transect T2. The transect intersects a bedrock outcrop at approximately 20m which is used to correlate to the bedrock radar facies (RF-2). Sublinear moveout features (F1) centered at approximately 42m have apparent velocity 0.15 m/ns, and are interpreted to be a conjugate set of bedrock fractures. b) Instantaneous amplitude plot of GPR transect T2. Areas of high amplitude are shown in red, medium amplitude in white and low amplitude in blue. High amplitude reflective areas are interpreted to represent sediment. Low reflectivity regions are interpreted as bedrock. 28

Figure 13. - Bedrock surface contour map with bedrock fractures. Elevations are reported relative to the water level of East Glacier Lake (3,282m amsl). Fractures F1 and F2 are resolved in two dimensions and therefore plotted in their actual orientation. Orientations of fractures F3 – F7 are unknown. They are plotted perpendicular to their radar transects. 31

Figure 14. - Excerpt from GPR transect T6 showing example of hyperbolic fit to the F2 sublinear feature. The apparent velocity determined from the hyperbolic fit is 0.15 m/ns. 32

Figure 15. - Interpreted GPR transect T6. The fracture (F2) shown in red appears to propagate into the sediment overburden. 33

Figure 16. - Soil classification triangle showing relationship between particle size and specific yield (modified from Johnson, 1967). 36

1. Introduction

In 1989 the Glacier Lakes Ecosystem Experiment Site (GLEES), located in the Snowy Range of southern Wyoming, was designated by the USDA Forest Service as a study site to examine the effects of atmospheric deposition on alpine and subalpine ecosystems (Musselman et al., 1992) (Figure 1). The site is comprised of three alpine lakes: Lost Lake, East Glacier Lake and West Glacier Lake and their associated watersheds (Figure 2).

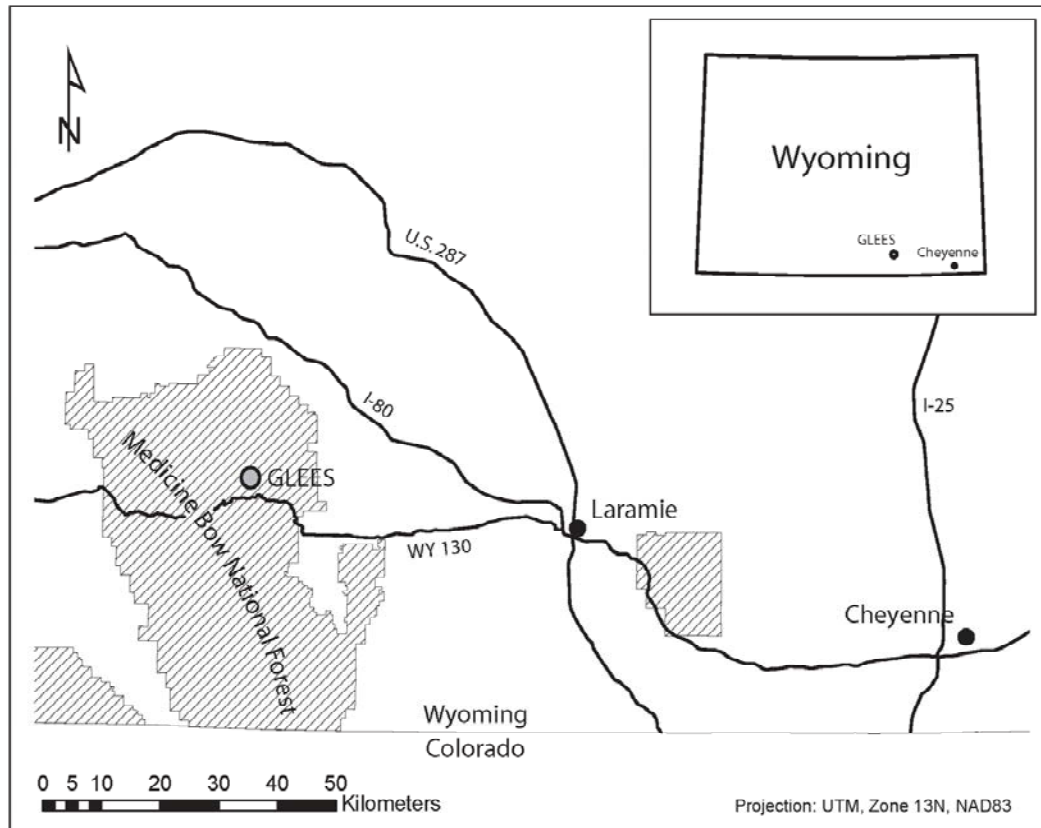


Figure 1. - Geographical location of GLEES.

The potential for groundwater storage and flow in the Glacier Lakes area is unknown because the thickness and hydrogeologic properties of the sediment overlying the bedrock are unknown (Hasfurther et al., 1992). In addition, the density and

interconnectivity of fractures in the bedrock beneath the site are unknown. An interconnected, dense fracture network in the bedrock could provide significant groundwater storage and provide conduits for groundwater flow.

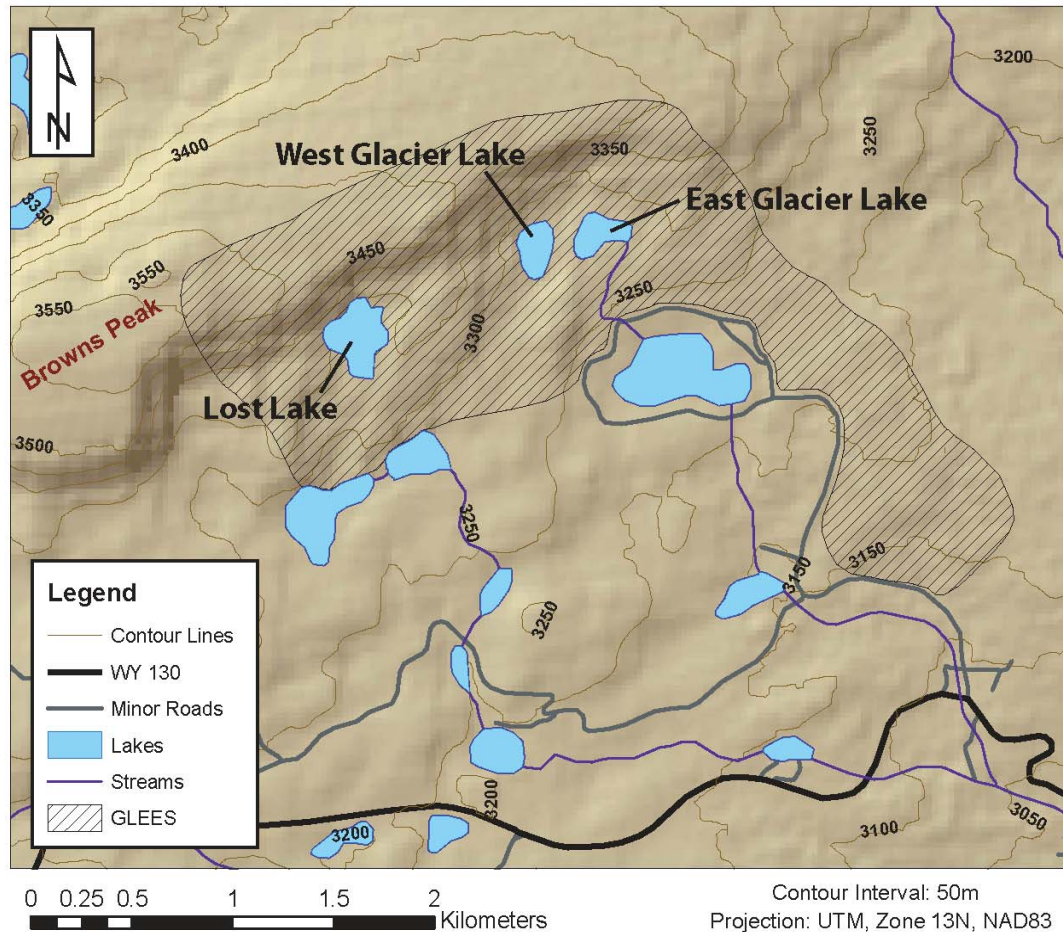


Figure 2. - Regional map of GLEES. Outline of GLEES from Musselman et al. (1992). Digital elevation model obtained from the Wyoming Geographic Information Science Center (<http://www.uwyo.edu/wygisc>).

The objective of this study is to use ground penetrating radar (GPR) to characterize the subsurface in portions of the watershed around East Glacier Lake (Figure 2). These radar data were used to create an isochore map of sediment geometry and a bedrock fracture map from which a volume of sediment and potential groundwater storage was estimated. In addition, the approximate annual groundwater discharge from

the sediment aquifer in the area of the outlet stream was estimated using Darcy's Law. A secondary objective is to obtain an estimate of bedrock fracture density and orientation as a preliminary step toward assessing the role of groundwater storage and flow in the bedrock. The results of this study will lead to an improved understanding of the subsurface geology at GLEES that will facilitate future studies of the role that groundwater plays in the water budget of the Glacier Lakes watershed. A better understanding of the groundwater system at GLEES will enable quantitative analyses of the groundwater chemistry involving the interaction and movement of anthropogenic pollutants among different components of the ecosystem (Musselman et al., 1992). This analysis is critical to the construction of models that can accurately predict the response of the watershed system to potential changes in physical or chemical environment which will aid in management decisions for GLEES and similar ecological zones throughout the Rocky Mountain west (Musselman et al., 1992).

The hypotheses to be tested in this paper are 1) that there is sufficient sediment volume and geometry to accommodate groundwater flow that is significant to the water budget of East Glacier Lake watershed, 2) the bedrock is fractured enough to transmit groundwater flow that is significant to the water budget, or 3) there is both enough sediment thickness and a fractured bedrock network that in tandem accommodate groundwater flow that is significant to the water budget.

2. Description of GLEES

GLEES is located in south central Wyoming on the Medicine Bow National Forest. The site is approximately 50 km west of Laramie, WY located north of State Highway 130 in the Snowy Range of Wyoming (Figure 1).

GLEES encompasses approximately 600 ha nestled in glacial cirques to the southeast of a SW – NE trending ridge extending eastward from Browns Peak (Figure 2) (Musselman et al., 1992). The site ranges in elevation from approximately 3,200 – 3,500 m above mean sea level (amsl). Three alpine lakes and their associated watersheds make up the upper portion of GLEES. The lakes are Lost Lake (6.7 ha), West Glacier Lake (3.3 ha) and East Glacier Lake (2.9 ha) with watershed areas of 51.4, 60.7, and 28.7 ha respectively (Musselman et al., 1992). This study focused on the area immediately surrounding East Glacier Lake, its outlet stream to the east and the area between East and West Glacier Lakes.

East and West Glacier Lakes were formed approximately 10,000 years ago during the last glacial episode probably by ice scour and moraine deposition (Vertucci and Conrad, 1992). These two lakes are of similar size and depth and are separated by an approximately N – S trending bedrock ridge that ranges in width from approximately 100 to 150 m.

East Glacier Lake covers an area of approximately 29,000 m², has a maximum depth of 7.0 m and contains an approximate water volume of 41,000 m³ (Vertucci and Conrad, 1992). The lake surface elevation is approximately 3,282 m amsl. East Glacier Lake has no perennial streams associated with it. Most of the contributing watershed to East Glacier Lake is to the north of the lake, and there are no well developed stream channels. Large areas of wet meadow along the eastern edge of East Glacier Lake during spring snowmelt suggest dispersed surface and sub-surface flow into the lake (Musselman et al., 1992). East Glacier Lake has an outflow channel which flows from the southeast corner of the lake at first diffusely through talus then becoming a well

defined single stream channel downstream. The outflow stream is gauged by a Parshall flume gauge which was installed in 1987 (Hasfurther et al., 1992). A hypolon liner was installed with the flume gauge to direct groundwater towards the surface to be measured as discharge. With no permanent snowfield in the East Glacier Lake watershed the outlet stream flows only until melt of the winter snowpack is complete (Hasfurther et al., 1992).

West Glacier Lake covers an area of approximately 33,000 m², has a maximum depth of 8.5 m and contains an approximate water volume of 45,000 m³ (Vertucci and Conrad, 1992). The lake surface elevation is approximately 3,276 m amsl. West Glacier Lake has four well defined inlet streams two of which are fed by meltwater from a permanent snowfield. As a result water flows into and out of West Glacier Lake perennially. The flow into West Glacier Lake is monitored with Parshall flume gauges, installed in 1987, on two of the inlet streams. West Glacier Lake has one outlet stream which flows from the south end of the lake. The outlet stream is gauged by a Parshall flume gauge, installed in 1986 (Hasfurther et al., 1992).

Ground cover at GLEES is subalpine forest and meadow with little to no vegetation in the higher elevations. The upper portion of GLEES, where the alpine lakes are located, consists of disconnected stands of evergreen forest intermingled with sparsely vegetated to barren meadows. Talus slopes are common.

The bedrock at GLEES is dominantly Precambrian Medicine Peak Quartzite with occasional mafic dike intrusions (Rochette, 1992). According to Rochette (1992) the mafic dikes make up approximately 15 – 20% of the bedrock in the Lost Lake and Glacier Lakes watersheds, but no mafic dikes are evident within the study area. Throughout GLEES the quartzite bedrock is extensively fractured in outcrop.

The Snowy Range of Wyoming was sculpted to its present morphology by Quaternary and Holocene glaciation (Rochette, 1992). Till in the GLEES area is thought to be of late Pinedale age so soil development probably began approximately 10,000 bp (Rochette, 1992). The surficial geology at GLEES is a poorly sorted sediment composed dominantly of quartzite boulders and cobbles derived from the Medicine Peak Quartzite bedrock. These boulders and cobbles have been left behind by glaciers as till and since by colluvial and alluvial processes such as freeze-thaw mechanical weathering of bedrock outcrops (Rochette, 1992). Throughout most of the site these quartzite boulders and cobbles are surrounded by a matrix of gravel, sand, silt and clay sized particles, probably of similar origin. However, there is evidence suggesting that fines in some portions of the site have been transported onsite by eolian processes (Hopper and Walthall, 1992).

Hopper and Walthall (1992) classified and mapped the poorly developed soils at GLEES using soil pedon classifications completed to approximately 1 m depth (Figure 3). Each soil pedon analysis included a grain size analyses based on sand, silt and clay percentages, ignoring larger material such as gravel, cobbles and boulders. The soils within the study area around East Glacier Lake include Typic Cryoboralfs, Dystric Cryochrepts, Lithic Cryochrepts and Typic Cryumbrepts (Hopper and Walthall, 1992). Talus, or areas of quartzite boulders and cobbles devoid of soil, termed Rubbleland by Hopper and Walthall (1992), are also present at GLEES. One such area is located in the vicinity of the East Glacier Lake outlet stream within the study site (Figure 3).

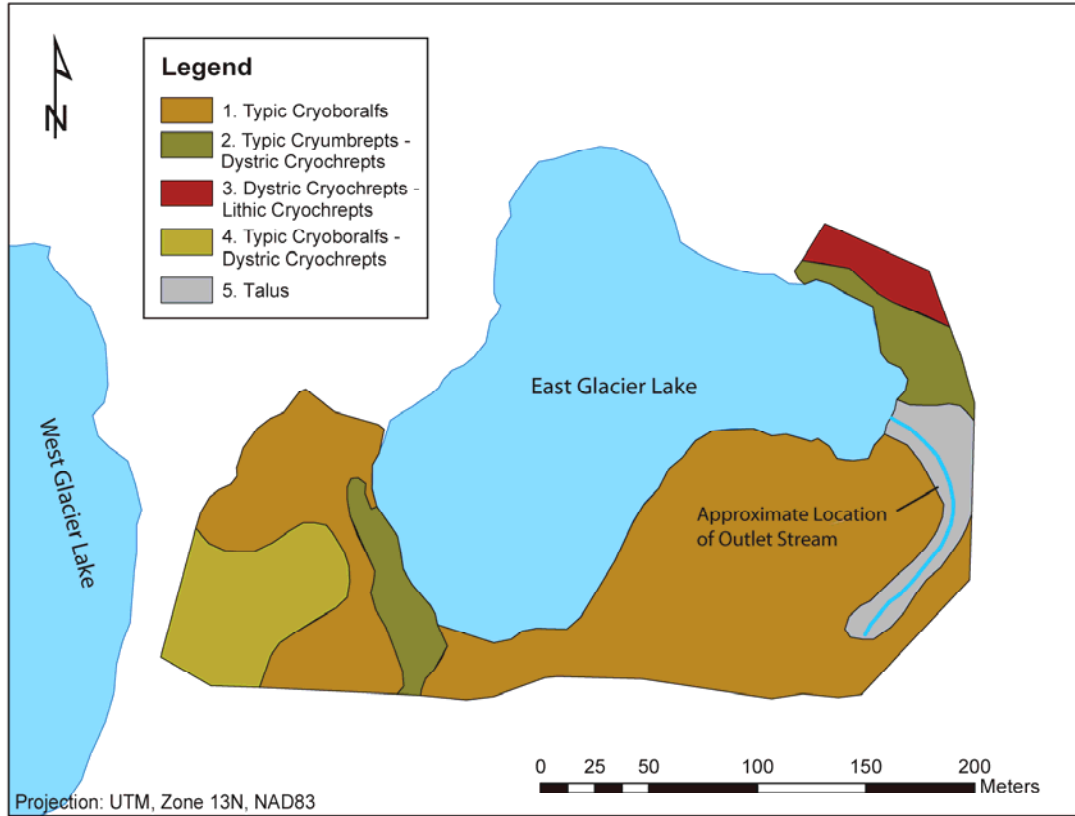


Figure 3. - Soil type map of study area (modified from Hopper and Walthall, 1992).

3. Previous Work

The water budget of East and West Glacier Lakes was initially studied by Hasfurther et al. (1992) and has been refined with work by Stednick (personal comm., 2010). The water balance equation used to evaluate water budgets within GLEES is:

$$\Delta S = P - (Q_{str,out} + Q_{gw,out} + ET + Es) \quad (1)$$

where ΔS is change in storage, P is precipitation, $Q_{str,out}$ is surface water discharge, $Q_{gw,out}$ is groundwater discharge, ET is evapotranspiration, and Es is snowpack sublimation. The parameters P , $Q_{str,out}$, ET , and Es are well documented for the East

Glacier Lake watershed; annual $P = 3.56 \times 10^5 \text{ m}^3$, $Q_{str,out} = 2.58 \times 10^5 \text{ m}^3$, $ET = 6.60 \times 10^5 \text{ m}^3$ and $E_s = 7.18 \times 10^5 \text{ m}^3$ (Stednick, personal comm. 2010). On an annual basis ΔS is considered to be essentially zero, but potential seasonal ΔS due to $Q_{gw,out}$ has not been investigated. Meteorological data including wind speed, wind direction, relative humidity, air temperature, soil temperature and precipitation has been collected at GLEES since 1987 and surface water discharge has been monitored by Parshall flume gauges in the East and West Glacier Lake watersheds (Musselman et al., 1992).

The original water budget study at GLEES for the East and West Glacier Lakes watersheds did not balance (Hasfurther et al, 1992). An error analysis indicated that the largest sources of error in the water budget were likely to be unaccounted input from the large permanent snowfield in the West Glacier Lake watershed and an unknown amount of groundwater inflow or outflow (Hasfurther et al, 1992). The big question involving groundwater is how much may be entering or leaving the watersheds, specifically whether there is seepage from East Glacier Lake into West Glacier Lake and if there is groundwater movement in the watershed (Hasfurther et al., 1992).

Work done on the permanent snowfield in West Glacier Lake watershed found that the permanent snowfield does not contribute a significant input to the water budget (Hultstrand, 2006). For the 2005 water budget the permanent snowfield was found to contribute less than 5% of the surface water discharge (Hultstrand, 2006). This observation led to subsequent work resulting in a recalibration of both the East and West Glacier Lakes outlet stream flume gauges. The refined flume gauge calibrations indicate that far less surface water discharge flows out of the watersheds than indicated in the

original water budget, bringing the water budget much closer to closing (Stednick, personal comm., 2010). Nonetheless, the groundwater component question remains.

Results from a seismic refraction survey suggested that unconsolidated materials overlie bedrock in the East and West Glacier Lakes watersheds to depths ranging from 0 to approximately 10 meters below ground surface (bgs) (Hasfurther et al., 1992). The seismic velocities of the sediment and bedrock were not as distinct as expected (approximately 245 – 2,900 and 1,800 – 5,600 m/s respectively), possibly indicating unconsolidated material deposited on a highly fractured regolith near the bedrock surface (Hasfurther et al., 1992).

4. Methods

4.1 Theory

Ground Penetrating Radar (GPR) is a non-invasive, portable and fast method of investigating the subsurface. Because of this, GPR is an ideal tool for use in remote, delicate environments such as the alpine to sub-alpine ecological zone (e.g. Leopold et al., 2008; Degenhardt et al., 2003). GPR has been used to image sedimentary stratigraphy (e.g. Davis and Annan, 1989; Beres and Haeni, 1991; Jol and Smith, 1991; van Overmeeren, 1998), the water table (e.g. Davis and Annan, 1989; Beres and Haeni, 1991; Annan et al, 1991), and to determine internal structures of sedimentary packages such as rock glaciers, alluvial fans and alpine talus deposits (e.g. Berthling et al., 2000; Ekes and Hickin, 2001; Degenhardt et al., 2003; Sass, 2006; Monnier et al., 2008). It has also been used to determine the interface between bedrock and sedimentary overburden (e.g. Collins et al., 1989; Davis and Annan, 1989; Sass, 2006) and to locate fractures in bedrock (e.g. Davis and Annan, 1989).

Ground penetrating radar (GPR) uses a short, high frequency electromagnetic pulse of energy propagated into the ground. The pulse is reflected back to the surface upon encountering inhomogeneities in subsurface electrical properties (Beres and Haeni, 1991). The dominant electrical properties that effect propagation and reflection of the radar wave are dielectric permittivity (ϵ) and electrical conductivity (σ) (Neal, 2004).

Dielectric permittivity (ϵ), a capacitive property, is the measure of a material's ability to store an electrical charge and is the dominant factor in controlling the propagation velocity of the radar wave in non-magnetic (low-loss) geologic materials (Neal, 2004). It is usually presented as a unitless value (relative dielectric permittivity, ϵ_r) normalized to the dielectric permittivity of free space ($\epsilon_0 = 8.86 \times 10^{-12} \text{ Fm}^{-1}$). Water has a high relative dielectric permittivity in comparison to air and typical rock forming minerals (Table 1), therefore water content in the subsurface exerts a primary control over variations in radar velocity (Neal, 2004). This relationship, for low-loss geologic materials, is:

$$v = \frac{c}{\sqrt{\epsilon_r}} \quad (2)$$

where v is radar velocity and c is the speed of light in a vacuum ($3.0 \times 10^8 \text{ m/s}$).

Electrical conductivity (σ) is the measure of a material's ability to transport an electric charge and is a significant factor in controlling attenuation of the radar wave (Neal, 2004). For typical geologic materials attenuation of the radar wave due to conduction increases with increasing frequency below a cut-off frequency of 10 – 300 MHz (Neal, 2004). Above this cut-off frequency attenuation of the radar wave due to

conduction becomes frequency independent and instead radar signal scattering becomes the dominant frequency dependent attenuation factor, especially as the radar wavelength approaches the size of the particles comprising the surveyed medium (Neal, 2004).

Attenuation of the radar wave is also related to geometric spreading (Neal, 2004, Beres and Haeni, 1991). In a homogenous material, as the radar wave propagates from the transmitting antenna it spreads in an ever-expanding sphere, causing the amplitude (A) of the signal to decrease as the inverse square of distance travelled:

$$A = A_0 e^{-\alpha z} \quad (3)$$

where A_0 is the initial radar signal amplitude, α is the radar attenuation constant and z is the distance travelled (Neal, 2004). For low-loss materials the radar attenuation constant (α) follows the relationship:

$$\alpha = \frac{\sigma}{2} \sqrt{\mu/\epsilon} \quad (4)$$

where μ is magnetic permeability, the measure of magnetic field energy stored and lost through induced magnetization (Neal, 2004). Alpha is frequency dependent because ϵ is frequency dependent. At high radar frequencies ϵ values are smaller, therefore high frequency radar waves are attenuated more rapidly than low frequency radar waves. For low-loss materials μ is approximately 1 (Neal, 2004). Generally the higher the electrical conductivity, the higher the attenuation factor, this is especially noted in saline water and

certain clay minerals (Neal, 2004). Table 1 shows a range of typical attenuation factor values for some common materials.

Table 1. - Common values for relative dielectric permittivity, electromagnetic wave velocity, conductivity and attenuation in associated geologic mediums (modified from Neal, 2004).

Medium	Relative dielectric permittivity (ϵ_r)	Electromagnetic-wave velocity (m/ns)	Conductivity (mS/m)	Attenuation (dB/m)
Air	1	0.3	0	0
Distilled water	80	0.03	0.01	2×10^3
Fresh water	80	0.03	0.5	0.1
Seawater	80	0.01	30000	1000
Unsaturated sand	2.55 - 7.5	0.1 - 0.2	0.01	0.01 - 0.14
Saturated sand	20 - 31.6	0.05 - 0.08	0.1 - 1	0.03 - 0.5
Unsaturated sand and gravel	3.5 - 6.5	0.09 - 0.13	0.0007 - 0.06	0.01 - 0.1
Saturated sand and gravel	15.5 - 17.5	0.06	0.7 - 9	0.03 - 0.5
Unsaturated silt	2.5 - 5	0.09 - 0.12	1 - 100	1 - 300
Saturated silt	22 - 30	0.05 - 0.07	100	1 - 300
Unsaturated clay	2.5 - 5	0.09 - 0.12	2 - 20	0.28 - 300
Saturated clay	15 - 40	0.05 - 0.07	20 - 1000	0.28 - 300
Unsaturated till	7.4 - 21.1	0.1 - 0.12	2.5 - 10	
Saturated till	24 - 34	0.1 - 0.12	2 - 5	
Limestone	4 - 8	0.12	0.5 - 2	0.4 - 1
Shales	5 - 15	0.09	1 - 100	1 - 100
Granite	4 - 6	0.13	0.01 - 1	0.01 - 1

Reflections of the radar wave are caused by contrasts in relative dielectric permittivities between subsurface units. The strength of the reflection is proportional to the magnitude of change in dielectric permittivity between units such that:

$$R = \frac{\sqrt{\epsilon_{r2}} - \sqrt{\epsilon_{r1}}}{\sqrt{\epsilon_{r2}} + \sqrt{\epsilon_{r1}}} \quad (5)$$

where R is the reflection coefficient and ϵ_{r1} and ϵ_{r2} are the relative dielectric permittivities of adjacent units 1 and 2 (Neal, 2004). Equation 4 assumes that contrasts in electrical conductivity between adjacent units are small (Neal, 2004). Typical values of

reflection coefficients for some common subsurface geologic interfaces are shown in Table 2.

Table 2. - Typical values of reflection coefficients for some common subsurface geologic interfaces. Values range from +1 to -1, the sign indicating polarity of the reflected wave (modified from Neal, 2004).

Layer 1 Layer 2	Porosity (%)	Relative dielectric permittivity (ϵ)	Reflection coefficient (+1 to -1)	Geological significance
Dry sand Saturated sand	35 35	3.1 20.7	-0.44	Water table
Dry sand Dry sand	35 30	3.1 3.27	-0.013	5% change in porosity
Saturated sand Saturated sand	35 30	20.7 17.7	+0.04	5% change in porosity
Round grains Platey grains	33 33	23.5 16.9	+0.08	Grain shape change
Isotropic grain packing Anisotropic grain packing	33 33	22.5 16.9	+0.7	Change in packing orientation

GPR frequencies (f) generally range from 50 – 1000 MHz. Survey frequency selection is guided by the tradeoff between resolution and depth of penetration. Resolution, or the ability of the GPR system to distinguish between two signals that are close together in time, is controlled by wavelength (Neal, 2004). The wavelength (λ) of the radar signal is:

$$\lambda = \frac{v}{f} \quad (6)$$

Generally the attenuation factor increases, or penetration depth decreases, as the radar frequency is increased and resolution increases as the radar frequency is increased (Davis

and Annan, 1989). The resolution of a GPR image is, in practice, approximately $\lambda/3$ to $\lambda/2$ (Beres and Haeni, 1991). For example, a 100 MHz radar wave traveling at 0.06 m/ns has a wavelength of 0.6 m. The resolution of this radar wave is therefore between 0.2 and 0.3 m. Some typical radar velocities and their associated mediums are shown in Table 1.

4.2 Field Protocol

GPR measurements were collected using a Sensors and Software[®] PulseEKKO[®] 100 system with 100 MHz antennas. The 100 MHz antennas proved to be a good compromise between penetration depth and resolution for this site (section 4.1). The survey was conducted along 12 transects in common offset step survey mode (Figure 4a) with a 1.0 m separation between the antennas and a step size of 0.25 m. The antenna separation and step size were selected to minimize the effects of electronic feedback between the antennas and to avoid spatial aliasing, respectively (Sensors and Software, 1999).

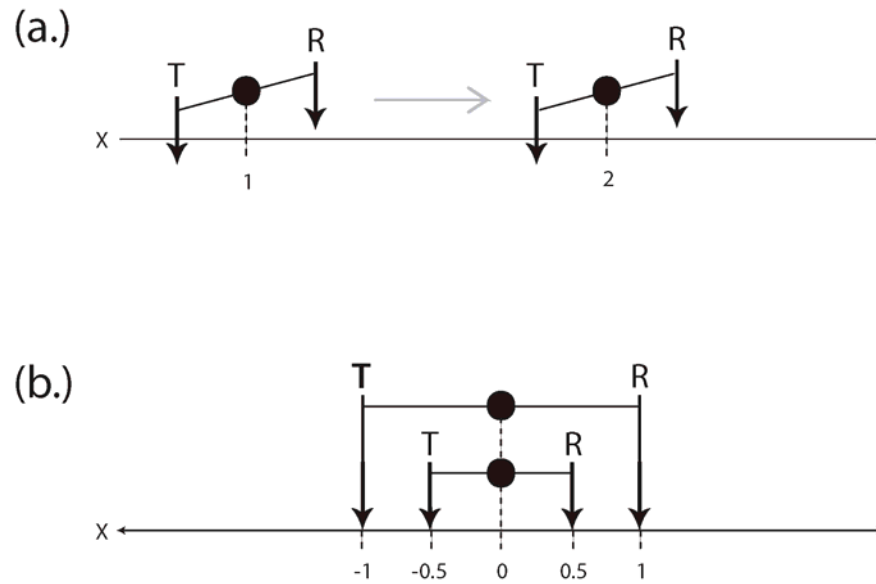


Figure 4. - a) Common offset survey mode: transmitting antenna (T) and receiving antenna (R) are held at a constant offset and stepped sequentially along the survey transect after each shot b) Common midpoint (CMP) survey mode: T and R are equally offset at greater distances apart following each shot. The midpoint between the two antennas remains constant and therefore remains the target of acquisition throughout the survey.

Each radar trace is the result of 64 stacks collected over a 500 ns time window. The result of “stacking” data, or taking the average of several (64) radar traces at each survey point, is an increase in the signal to noise ratio. This is because noise in the radar signal is usually random and tends to zero when averaged (Sensors and Software, 1999).

Assuming a nominal radar velocity of 0.1 m/ns (Table 1) a 500 ns time window will collect data up to 25 m bgs. Radar data was collected over a 0.8 ns sampling interval yielding a Nyquist frequency of 625 MHz. This is adequate to reproduce frequencies well above those recorded in the survey. Three longitudinal transects were oriented approximately N-S and nine transverse transects were oriented approximately E-W around East Glacier Lake (Figure 5).

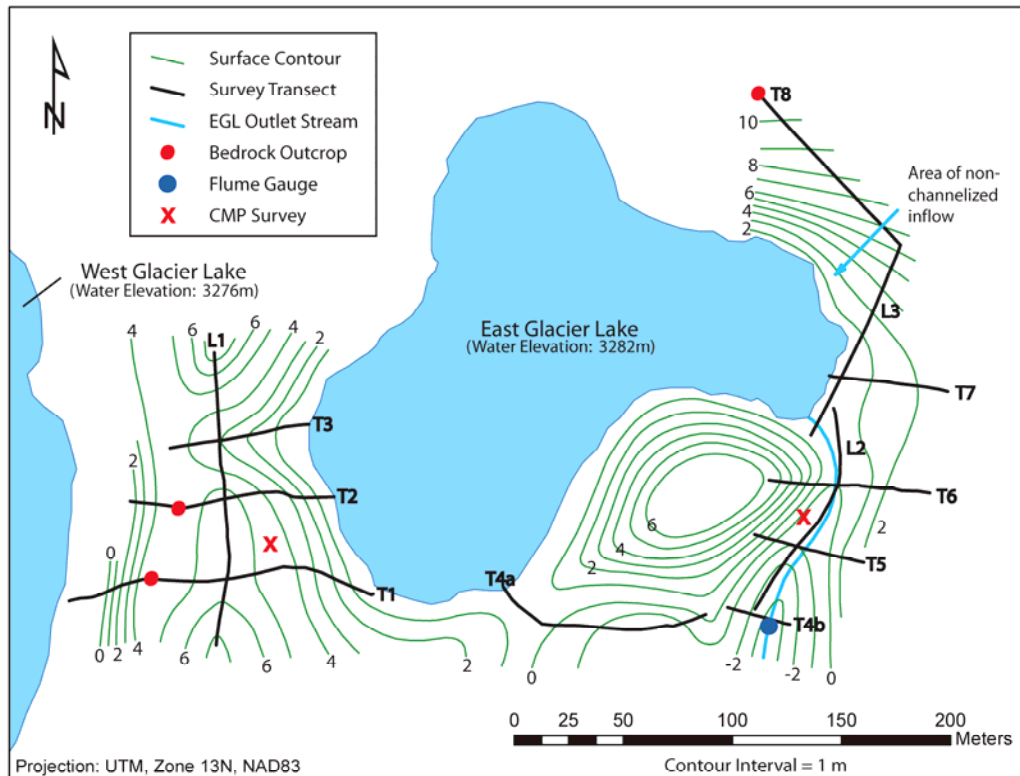


Figure 5. - Topographic study site map showing survey transect layout, bedrock outcrop locations, CMP survey locations and the location of the East Glacier Lake outlet stream Parshall flume gauge. Elevations are reported relative to the water level of East Glacier Lake (3,282m amsl). Two areas of interest were surveyed; the median between East and West Glacier Lakes (transects L1, T1, T2 and T3) and the area of non-channelized inflow and the outlet stream on the east side of East Glacier Lake (transects L2, L3, T4a, T4b, T5, T6, T7 and T8).

Two areas of interest were targeted, one on the east side of East Glacier Lake including both the area of non-channelized inflow to the lake and the outlet stream and the other on the divide between East and West Glacier Lakes. Transects were located such that three bedrock outcrops were intersected and five of the survey transects terminated at the edge of East Glacier Lake (Figure 5). This layout was designed to provide points of known bedrock and surface water to correlate with bedrock and the water table in the subsurface. Two common midpoint (CMP) surveys were also performed to determine average radar velocity in the subsurface (Figure 4b, Figure 5).

The relative locations and elevations of the survey transects were determined using a laser total station. Total station survey points were collected at endpoints of the survey transect, at recognized features such as rock outcrops or edge of water and at points of break in slope along the survey transects. The survey grid was located in UTM coordinates using a handheld GPS. GPS points were taken at the endpoints of each survey transect. The accuracy achieved with the laser total station is within ± 3 mm for distance and 6 seconds angularly. The GPS system used has a horizontal accuracy of 15 m (Garmin, 2003). Aerial photography was also used to aid in geo-referencing the survey grid.

The radar data were processed using Sensors and Software[®] EKKO_View Deluxe[®] version 1, release 3 (Sensors and Software, 2002 – 2007). The processing sequence showing effects of each processing step is shown in Figure 6. Two transects, L1 and T1, required merging of fragment transects. The two CMP surveys were analyzed to determine average radar velocity in the subsurface. Preliminary processing of the 12 GPR transects followed the methods described by Neal (2004), and included signal saturation correction (dewow) and an automatic re-pick of time zero to equally align all first breaks of the radar traces within each GPR transect. Deconvolution was then applied to reduce reverberation in the radar signal using the default EKKO_View Deluxe[®] parameters (frequency: 100 MHz, filter width: 30 ns, delay: 7.5 ns, spike width: 3 ns and whitening: 0.1). Other parameter values were tested, but did not improve the image. At this point diffraction hyperbolas in several of the radar transects were inspected for shape

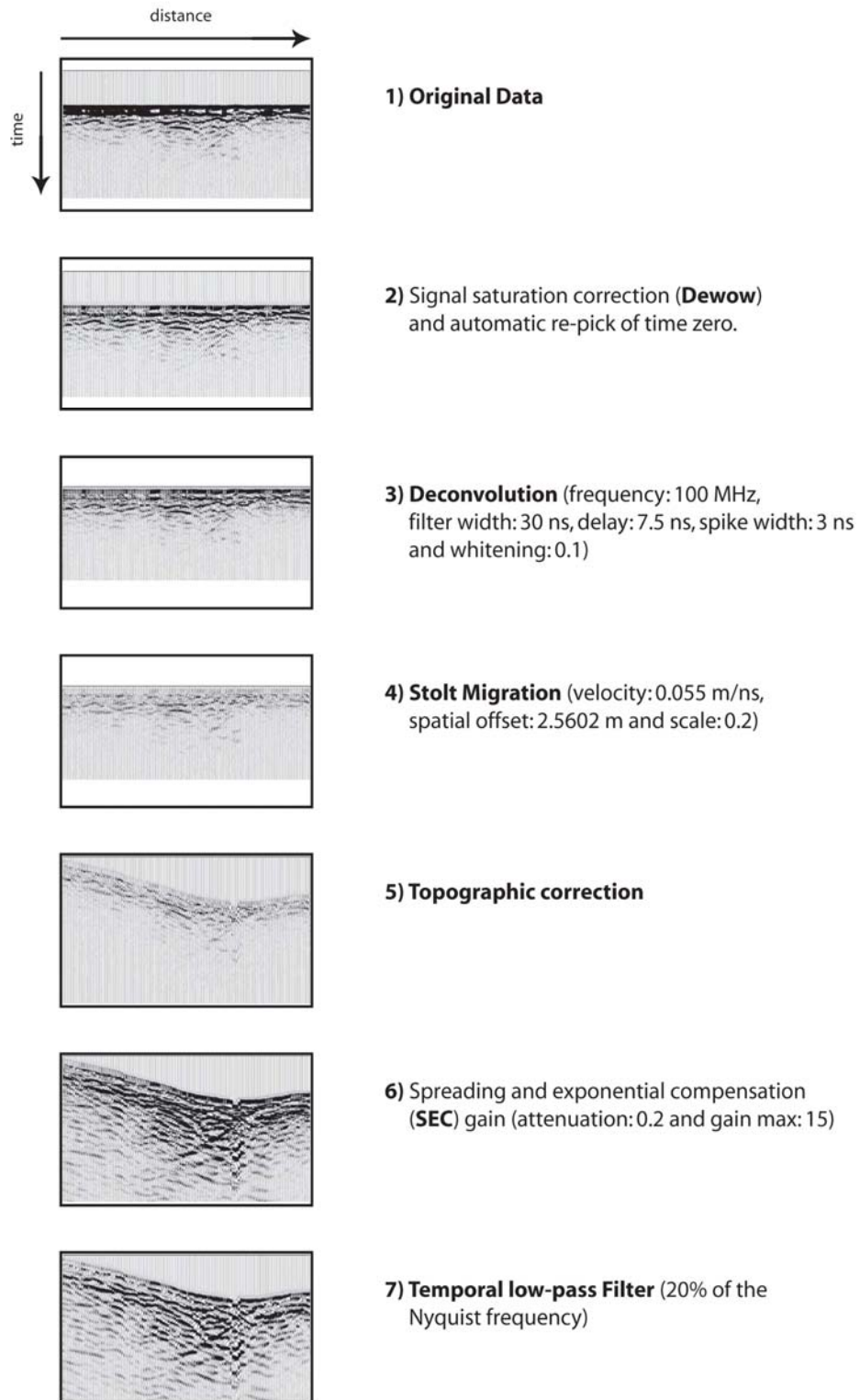


Figure 6. - Graphical illustration of the GPR processing sequence used in this study.

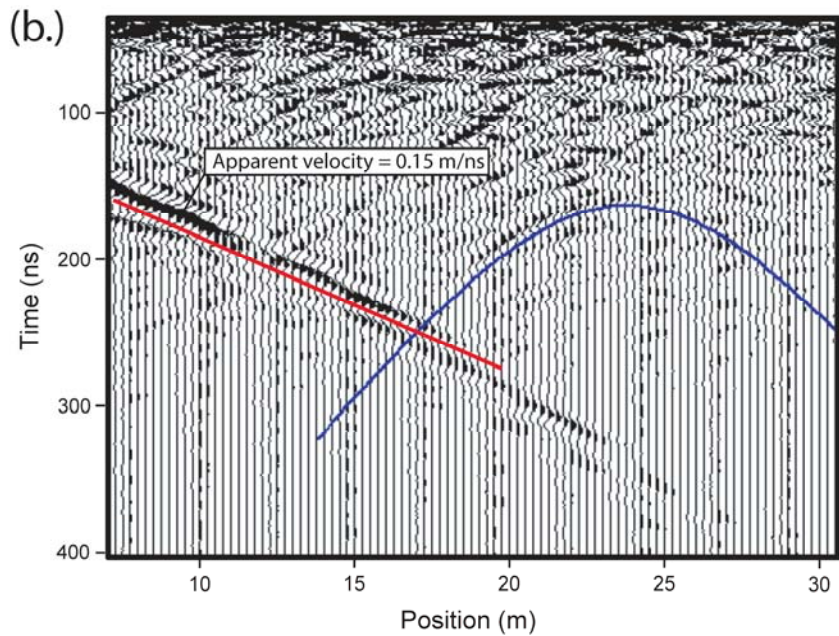
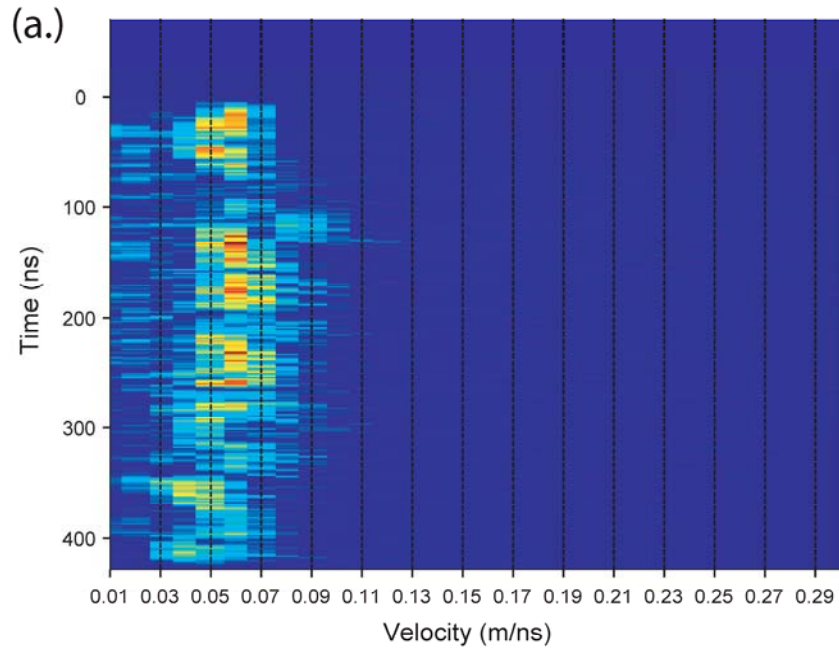


Figure 7. - a) Semblance analysis of the common midpoint (CMP) survey. The warmer colors indicate the most likely radar velocities. b) Example of comparison of hyperbolic fit to diffractions in the radar data. The average velocity determined from these analyses is 0.06m/ns. Note the strong sublinear moveout feature dipping to right with an apparent velocity of 0.15 m/ns. This is a feature from the subsurface.

to supplement and verify the average radar velocity (0.06 m/ns) determined from the CMP analysis (Figure 7). The hyperbola shapes indicated agreement with the average radar velocity determined with the CMP analyses. Stolt migration (Sensors and Software, 2003) using the parameters 0.055 m/ns velocity, 2.5602 m spatial offset (window width in meters used for the synthetic aperture process, default value used) and 0.2 scale (the synthetic aperture process tends to gain the data and the scale factor reduces this gain effect (Sensors and software, 2003)) was applied to the dataset to collapse these diffractions to their point sources, and then a topographic correction was applied. A spreading and exponential compensation (SEC) gain was applied to boost the amplitude of reflections in the dataset while maintaining relative signal strength (Sensors and Software, 2003). Parameter testing led to a choice of 0.2 attenuation and 15 gain max for the SEC gain. Finally, a temporal low-pass filter was applied to attenuate high frequency noise from the dataset using a cutoff percentage of 20% of the Nyquist frequency (cutoff above 125 MHz). This cutoff percentage was selected based on parameter testing and inspection of the average amplitude spectrum plots of the radar transects (Figure 8).

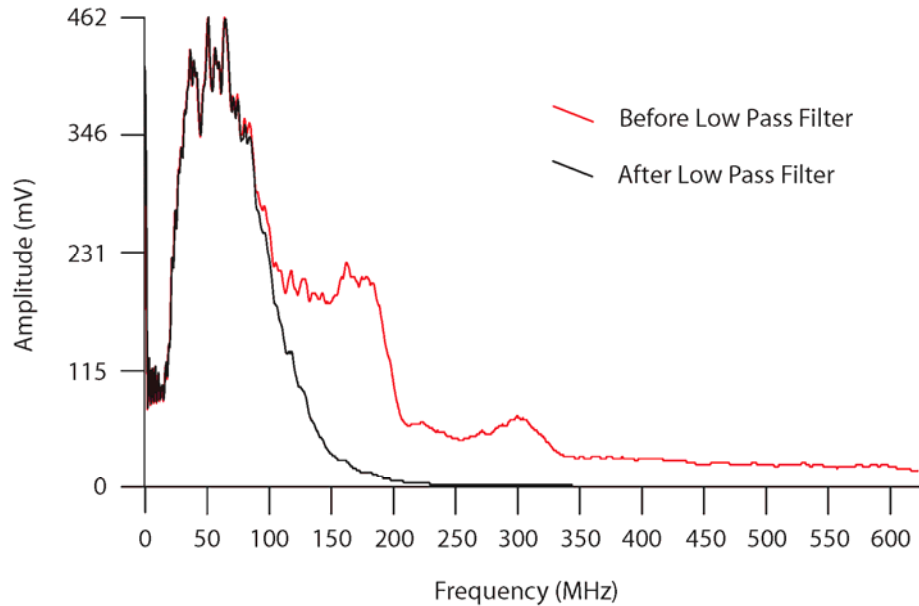


Figure 8. - The average amplitude spectrum plot for transect T2 before and after application of the temporal low-pass filter.

4.3 Radar Facies

In order to distinguish between different lithostratigraphic units, two radar facies were defined. A radar facies can be defined as a mappable three-dimensional subsurface unit composed of reflections that can be distinguished from adjacent units on the basis of shape, amplitude and continuity (Jol and Smith, 1991). The subsurface geology in the study area is known to be a quartzite bedrock overlain by a poorly sorted sediment composed of quartzite boulders and cobbles with intermingled fines (Rochette, 1992) (section 2). Two radar facies are recognized in the radar profiles at the study site. RF-1 is characterized by laterally continuous, high amplitude, sub-horizontal reflectors which

exhibit occasional pinchouts and onlap with lower facies (Figure 9a). RF-2 is characterized by a range from low amplitude, sub-horizontal reflectors with limited lateral continuity to reflection free (Figure 9b). Based on correlation at the surface radar facies RF-1 and RF-2 are interpreted to correspond to the sediment overburden and the quartzite bedrock, respectively. Also recognized in the radar profiles are features interpreted to be bedrock fractures, which appear as linearly dipping, laterally continuous, high amplitude, single reflections appearing dominantly in the RF-2 section of the profile, but occasionally extending into the RF-1 section.

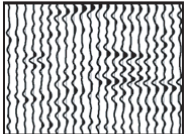
	Description	Interpretation
(a.) 	RF1 – Laterally continuous, high amplitude, sub-horizontal reflectors which exhibit occasional pinchout and onlap with lower facies.	<i>Sediment Overburden</i>
(b.) 	RF2 – Range from low amplitude, sub-horizontal reflectors with limited lateral continuity to reflection free.	<i>Bedrock</i>

Figure 9. - Description and geologic interpretation of the radar facies used in the interpretation of the GPR dataset.

4.4 Creating an Isochore Map

A bedrock surface map contoured at 1 m intervals was created from the radar data. Using the radar facies analysis described above the sediment-bedrock interface was picked along each of the 12 GPR transects at a 2.5 m interval. The bedrock outcrops intersected by transects T1, T2 and T8 (Figure 5) were used to correlate the surface expression of bedrock with the RF-2 (bedrock) facies. The water table was not recognized on any of the radar transects. Possible reasons for this are discussed below.

Two-way travel time to the sediment-bedrock interface picks were converted to depth using the average radar velocity (0.06 m/ns) determined from the CMP analysis. These depths were converted to elevations relative to the water level of East Glacier Lake (3,282 m amsl). These data were hand contoured using the interpretive contouring method described by Tearpock and Bischke (2003).

A surface topography map with 1 m contour intervals was created using data points collected from the total station survey of the survey transects. This map was also hand contoured using the interpretive contouring method and reported in elevations relative to the water level in East Glacier Lake.

An isochore map of sediment thickness was created via a conformable mapping technique (Tearpock and Bischke, 2003). Along the radar transects the sediment-bedrock interface elevation was subtracted from the land surface elevation at 2.5 m intervals. Additional data points located between the radar transects were created by overlaying the topographic land surface map and the bedrock surface contour map. Where a contour line from one map intersects a contour line from the other map the thickness of sediment at that point is determined by subtracting the bedrock surface value from the land surface topography.

4.5 Estimating Maximum Storage and $Q_{gw,out}$

As a first step toward estimating storage, the volume of sediment was estimated by integrating the isochore map using ArcGIS[®] 9.2 (ESRI, 2008). In an unconfined aquifer the product of aquifer volume and specific yield (S_y) approximates the amount of water that can be removed from storage during gravity drainage (Schwartz and Zhang, 2003).

Due to protections on the pristine nature of GLEES by the USDA Forest Service no sediment samples were collected for S_y laboratory analysis during this study so the soil type map from Hopper and Walthall (1992) was used to estimate S_y values. The survey area was broken into five different soil type regions (Figure 3), four of which are represented by a corresponding grain size analysis from Hopper and Walthall (1992). Average S_y values for these four soil types are based on these grain size analyses. The fifth soil type area in the study site is talus (Hopper and Walthall, 1992) and does not have a corresponding grain size analysis. The S_y value used for this area is based on material description.

Annual groundwater discharge in the area of the outlet stream was estimated with Darcy's Law using the approximate cross sectional area of the sediment aquifer at transect T4b, the approximate hydraulic gradient between the water level of East Glacier Lake and the ground surface elevation at the intersection of transects T4b and L2, and the average saturated hydraulic conductivity of the sediment aquifer determined by Houghton et al. (2011).

5. Results

The average radar velocity determined from the CMP analyses and inspection of diffractions on radar transects is 0.06 m/ns (Figure 7). The average radar velocity was used to convert the radar profiles from two way travel time to depth beneath the land surface. Sediment thickness determined from the radar data at the study site ranges from 0 m at bedrock outcrops to > 9 m near East Glacier Lake and averages approximately 2.5 m (Figure 10). Generally, sediment thickness increases toward East Glacier Lake abruptly within several meters of shore. Otherwise, the sediment overburden mimics

underlying bedrock topography with generally more thickness in the valleys than the ridges. One exception is an isolated deep pocket of sediment on the ridge between East and West Glacier Lakes located between 32 and 42 m along radar transect T1 (Figure 10). Here the sediment depth reaches > 5 meters within 5 meters laterally of a bedrock outcrop to the west. The total volume of sediment overburden represented by the isochore map is $83,800 \pm 8,400 \text{ m}^3$.

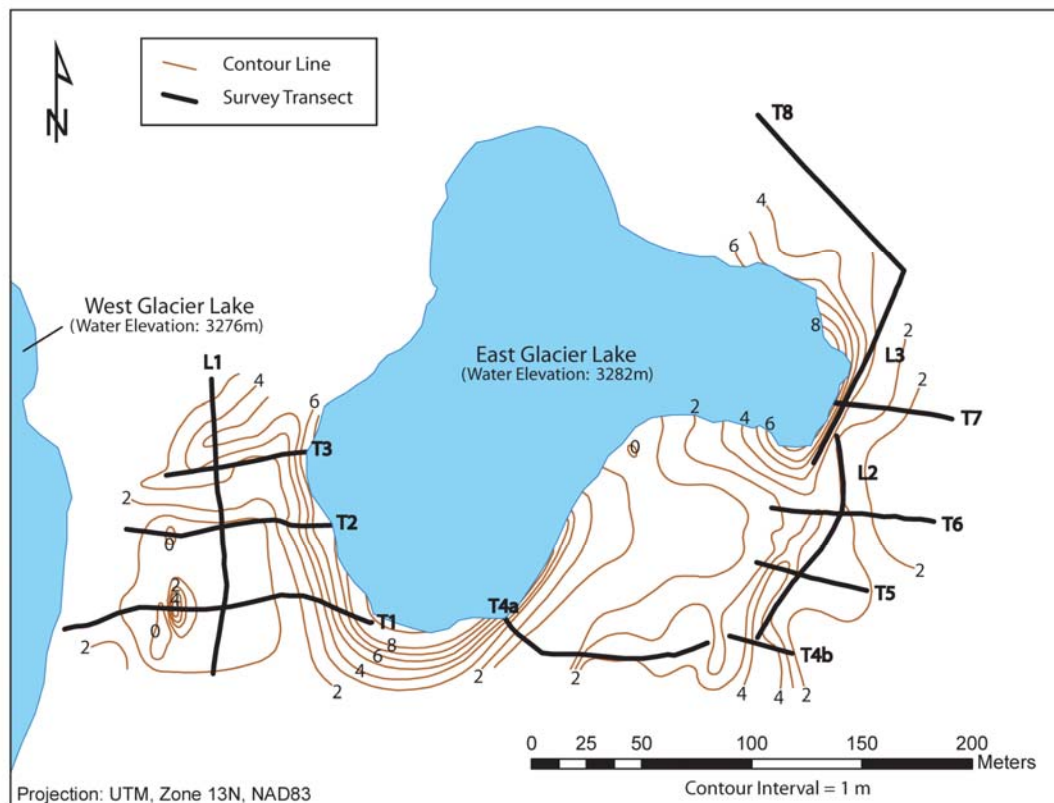


Figure 10. - Isochore map of sediment overburden. The contour lines represent sediment thickness. The sediment is generally thicker in valleys and thinner on ridges. Notice the isolated deep pocket of sediment located on transect T1.

Figure 11 shows the processed radar transect T2 in wiggle trace format. Each vertical wiggle trace represents a single GPR survey point along the transect.

Figure 11 - GPR transect T2. Elevation is relative to the water level of East Glacier Lake (3,282m amsl). Depths below ground level are based on an average radar velocity of 0.06 m/ns.

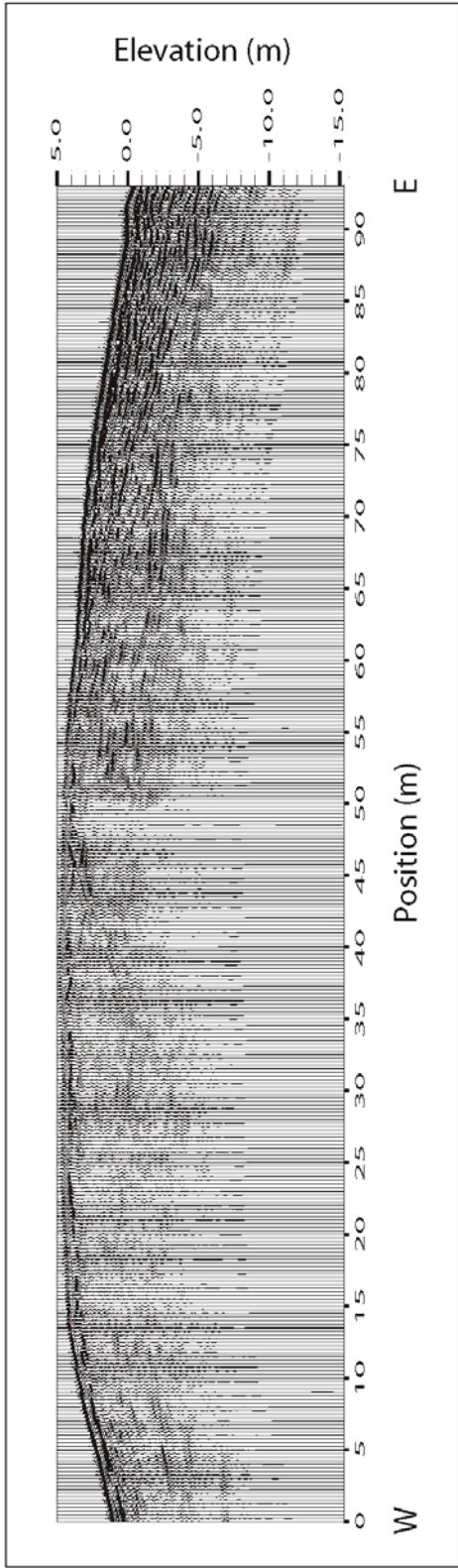
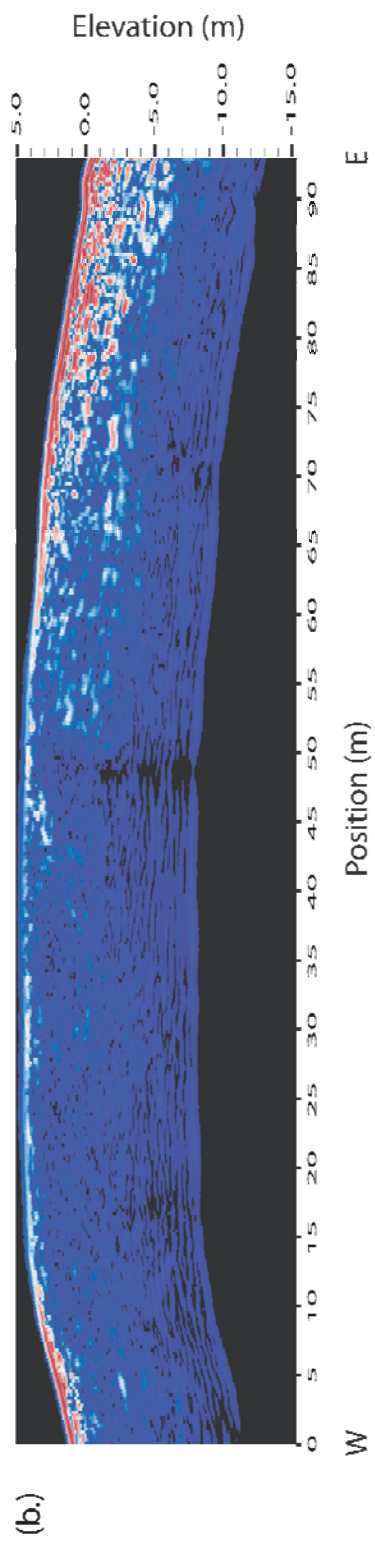
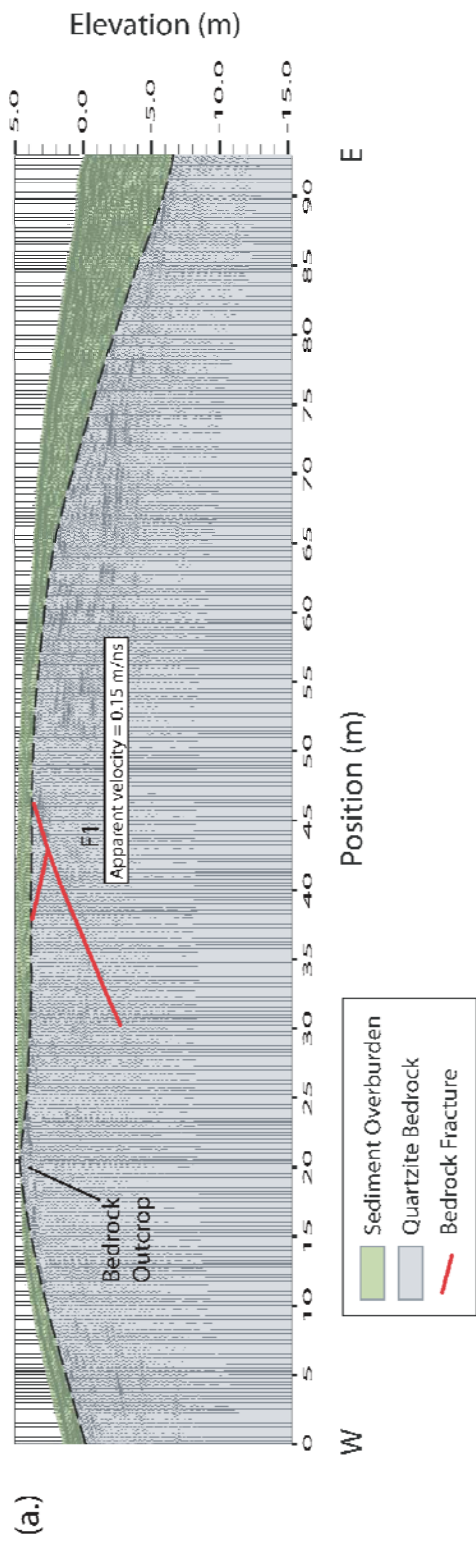


Figure 12 - a) Interpreted GPR transect T2. The transect intersects a bedrock outcrop at approximately 20m which is used to correlate to the bedrock radar facies (RF-2). Sublinear moveout features (F1) centered at approximately 42m have apparent velocity 0.15 m/ns, and are interpreted to be a conjugate set of bedrock fractures. b) Instantaneous amplitude plot of GPR transect T2. Areas of high amplitude are shown in red, medium amplitude in white and low amplitude in blue. High amplitude reflective areas are interpreted to represent sediment. Low reflectivity regions are interpreted as bedrock.



The interpreted wiggle trace radar transect T2 is shown in Figure 12a and an instantaneous amplitude plot of radar transect T2 is shown in Figure 12b for comparison. In radar transect T2 sediment thickness ranges from 0 m at the bedrock outcrop to approximately 7 m at the east end of the radar transect near East Glacier Lake. There is a bedrock outcrop at approximately 20 m which has been used to correlate to the bedrock radar facies RF-2. The high amplitude sublinear reflections centered at approximately 42m along the radar transect have an apparent velocity of 0.15 m/ns. This is too low to be an airwave reflection and is instead interpreted to be reflections from a conjugate set of bedrock fractures (F1). Appendix A contains processed wiggle trace and interpreted wiggle trace figures of each radar transect.

Bedrock fracturing is thought to be extensive, as evidenced in bedrock outcrops throughout GLEES (Rochette, 1992). Seven fractures were imaged in this survey, mostly on the east side of East Glacier Lake (Figure 13). Two of the fractures were imaged on more than one GPR line (F1 and F2), allowing determination of their strikes and dips. These are $N0^{\circ} E, 33^{\circ} W$ and $22^{\circ} E$ (conjugate set) and $N88.2^{\circ} E, 16.9^{\circ} N$ respectively. The other five fractures are plotted in Figure 13 with strikes assumed perpendicular to the radar transects.

Four of the fractures imaged (F1, F4, F5 and F7) are confined to the bedrock (e.g. F1, Figure 12a) while the other three fractures (F2, F3 and F6) propagate into the sediment overburden, as seen in radar transect T6 (e.g. F2, Figure 15). The two dimensional bedrock fracture density as resolved by this survey is approximately 1 fracture per $4,810 \text{ m}^2$.

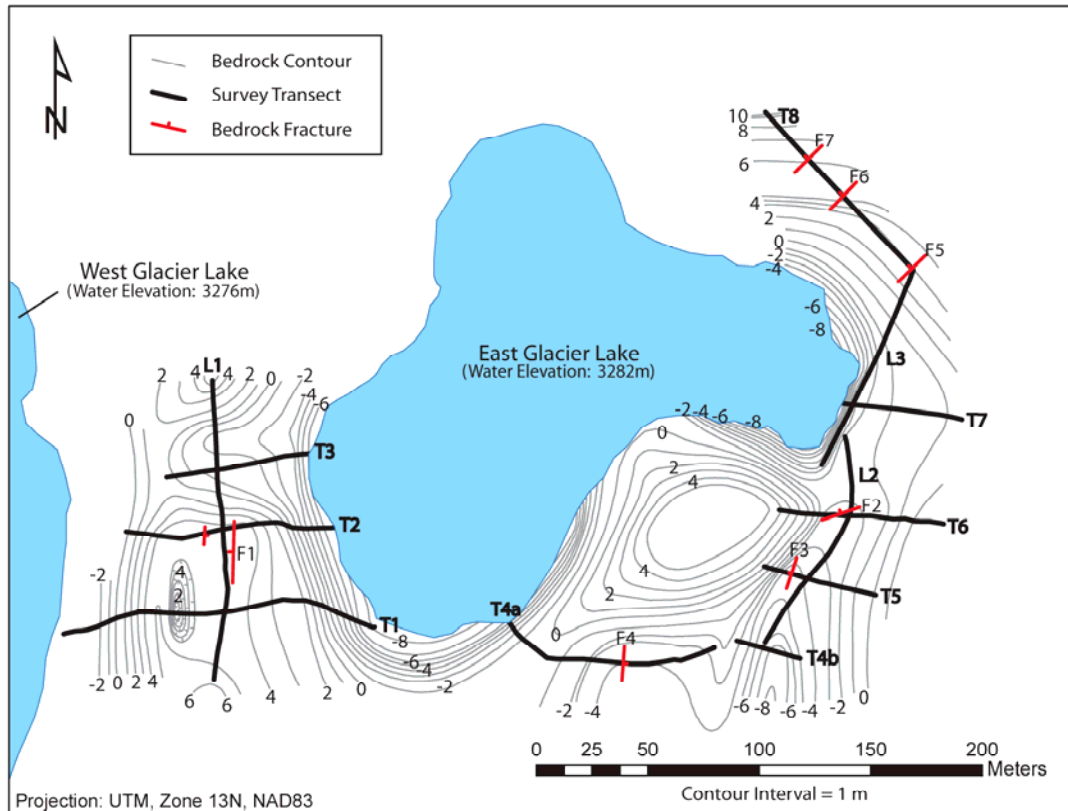


Figure 13. - Bedrock surface contour map with bedrock fractures. Elevations are reported relative to the water level of East Glacier Lake (3,282m amsl). Fractures F1 and F2 are resolved in two dimensions and therefore plotted in their actual orientation. Orientations of fractures F3 – F7 are unknown. They are plotted perpendicular to their radar transects.

The sublinear features that are considered to be bedrock fractures do not demonstrate either airwave velocity (0.3 m/ns) or direct ground-wave velocity (~0.06 m/ns in this terrain). The apparent velocities of sublinear features F1 through F7 range from 0.11 m/ns to 0.15 m/ns as determined from hyperbolic fit (e.g. Figure 14). Therefore, these features occur in the subsurface and are not ground-waves or artifacts of reflection from objects above the ground surface. The GPR signatures interpreted as bedrock fractures in this study are very similar to the bedrock fracture signatures found in the Davis and Annan (1989) GPR investigation conducted in a tunnel through granite.

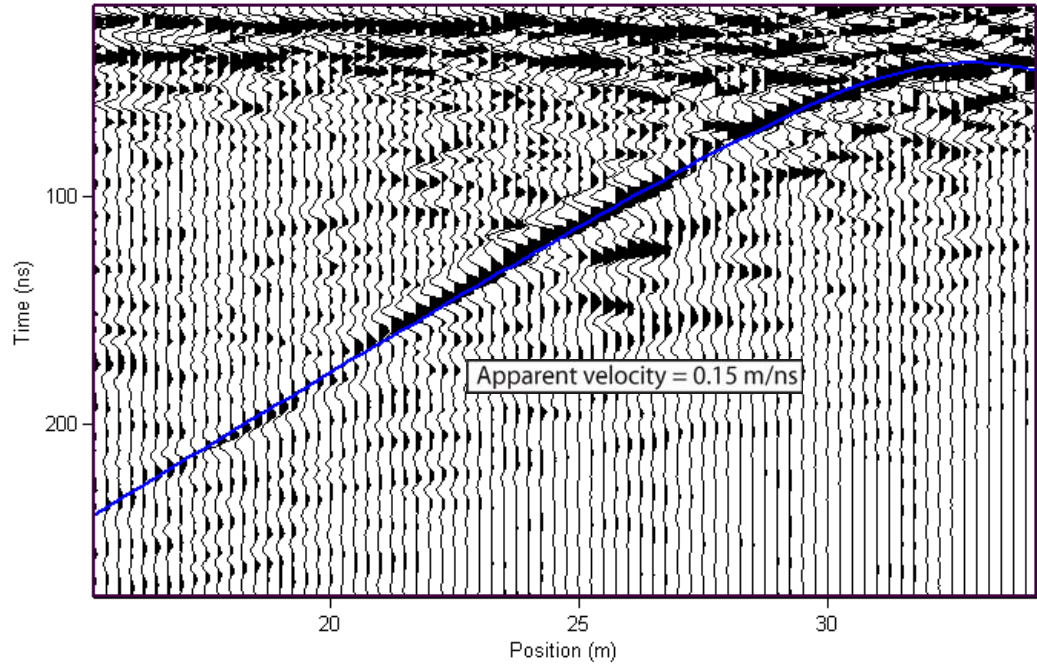
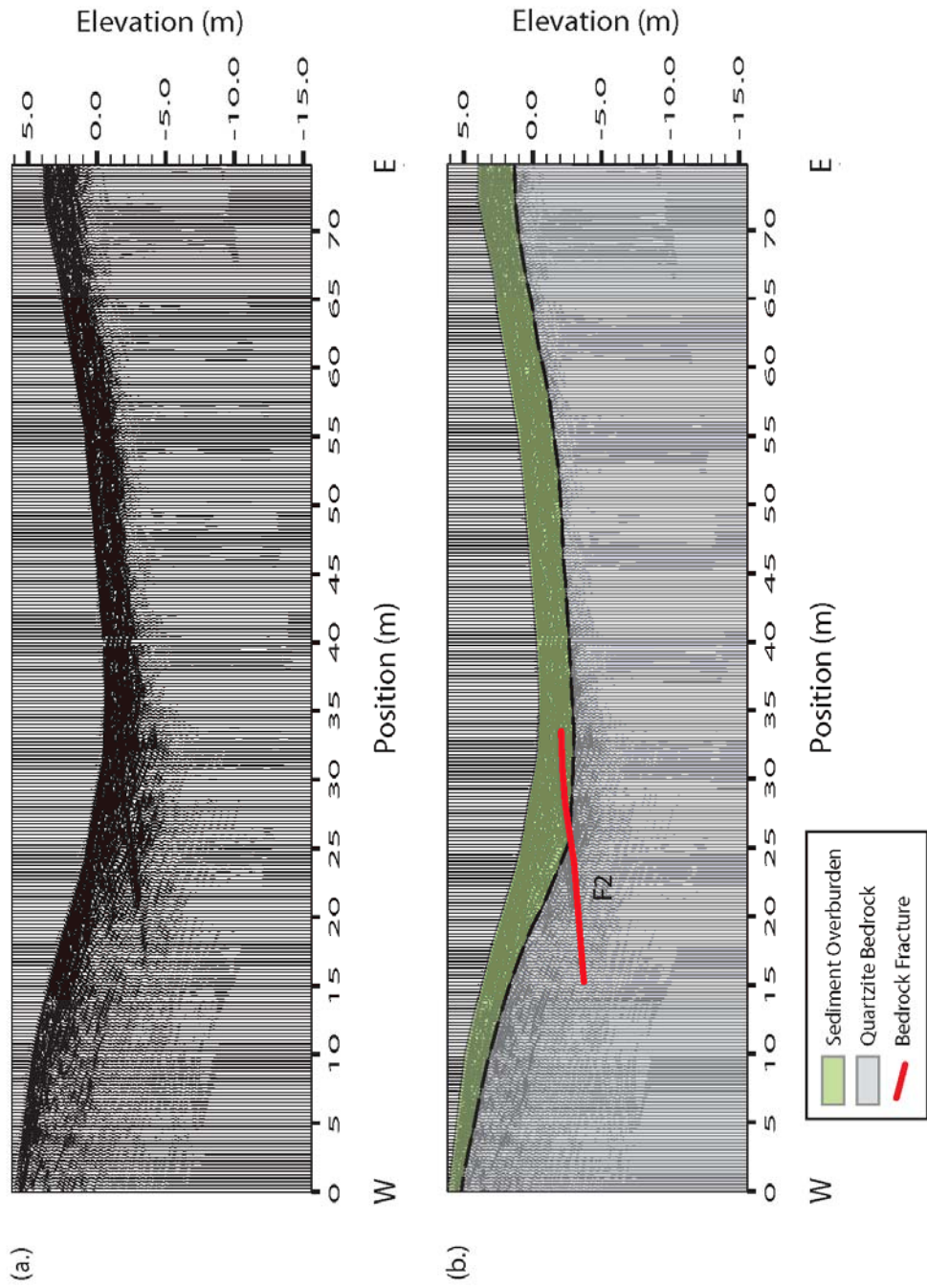


Figure 14. - Excerpt from GPR transect T6 showing example of hyperbolic fit to the F2 sublinear feature. The apparent velocity determined from the hyperbolic fit is 0.15 m/ns.

Figure 15 - Interpreted GPR transect T6. The fracture (F2) shown in red appears to propagate into the sediment overburden.



Average specific yield for the study site was calculated using an area weighted average grain size analysis based on the percent area of each soil type at the study site. The average grain size analysis for soil type regions 1 through 4 (A_{1-4} , 93% of study site area) is 45.1% sand, 33.5% silt and 21.4% clay (Fig. 3). This corresponds to a specific yield of approximately 9% as determined from the soil classification triangle relating particle size to specific yield (Figure 16, after Johnson, 1967). The specific yield for soil type region 5 (A_5 , 7% of study site area) was estimated to be 22% for boulders, cobbles and sand (Johnson, 1967). The overall average specific yield for the study site is equal to the area weighted average of specific yields for these two areas:

$$S_y = \frac{(A_{1-4} \times S_{yA_{1-4}}) + (A_5 \times S_{yA_5})}{100} = \frac{(93 \times 9) + (7 \times 22)}{100} \approx 10\% \quad (7)$$

where A_{1-4} and A_5 are the percent areas represented by soil type regions 1 through 4 and soil type region 5, respectively and $S_{yA_{1-4}}$ and S_{yA_5} are the specific yields estimated for soil type regions 1 through 4 and soil type region 5, respectively. The average specific yield for the study site is therefore approximately 10%.

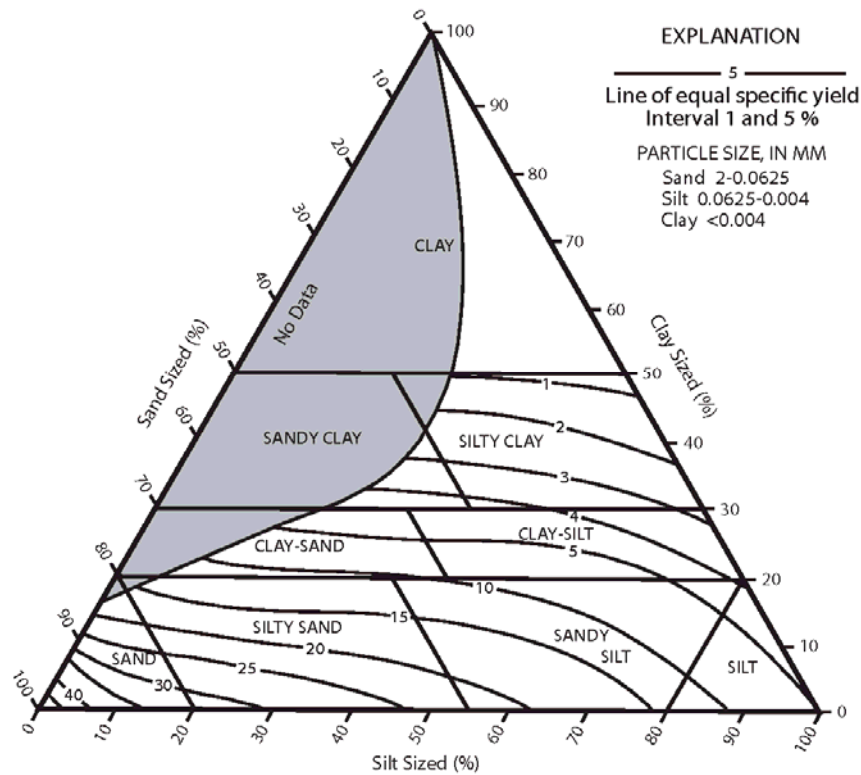


Figure 16. - Soil classification triangle showing relationship between particle size and specific yield (modified from Johnson, 1967).

Based on the specific yield estimate of 10% the maximum change in groundwater storage for the volume of sediment represented by the isochore map is 8,380 m³, assuming initial saturation followed by complete gravity drainage of the sediment aquifer. The study site covers an area of 33,700 m² while the area of the East Glacier Lake watershed, for which the water budget is calculated, is approximately 287,000 m². The study area therefore represents approximately 12% of the watershed area. If the sediment volume and average specific yield of the study area can be considered representative of the East Glacier Lake watershed as a whole, an estimate of the maximum potential change in groundwater storage for the watershed can be made. Based

on these assumptions the maximum potential change in groundwater storage for the entire East Glacier Lake watershed is 61,300 m³. This is approximately 17% of the average annual precipitation (356,000 m³) and approximately 24% of the average annual surface water discharge (258,000 m³) recorded for the East Glacier Lake watershed.

Annual groundwater discharge ($Q_{gw,out}$) in the area of the outlet stream was estimated using Darcy's Law:

$$Q_{gw,out} = K_s i A \quad (8)$$

where K_s is the average saturated hydraulic conductivity of the sediment aquifer, i is the hydraulic gradient as determined between the water level of East Glacier Lake at the outlet stream and the ground elevation at the intersection of transects T4b and L2 (Figure 5), and A is the cross sectional area of the sediment aquifer at transect T4b (Figure 5). K_s as determined based on infiltration tests conducted using a double-ring infiltrometer (Houghton et al., 2011) is 2.3 m/day, i is 3.40×10^{-2} , and A is approximately 110 m². Therefore the estimated annual groundwater discharge in the area of the outlet stream is approximately 3,140 m³.

6. Uncertainty

Sources of potential error in this study include uncertainty in the location of the interface between sediment overburden and bedrock estimated in the GPR transects, error associated with interpretive contouring (Tearpock and Bischke, 2003), propagation of these errors into calculation of the volume of the sediment overburden, error associated

with calculating the average specific yield within the aquifer, and scaling error associated with the assumption that the study site is representative of the watershed as a whole.

The interface between sediment and bedrock is not always distinct in a radar image (Sass, 2006). Because the dominant composition of the sediment overburden is quartzite derived from the underlying quartzite bedrock there is little dielectric contrast at the interface. Accordingly, in this study area the interface is usually characterized by a gradational decrease in reflectivity and change in reflection continuity rather than by one distinct reflection (see Sass, 2006 for discussion of a similar situation). The 100 MHz radar wave traveling at 0.06 m/ns has an effective vertical resolution of approximately 0.25 m ($\lambda/3$ to $\lambda/2$) which is the minimum bed thickness that can be resolved (Beres and Haeni, 1991). Picks of the sediment-bedrock interface along the radar transects are probably also within $\lambda/3$ to $\lambda/2$ or ± 0.25 m of the actual interface especially in locations where the interface is more gradational, corresponding to a highly weathered and fractured upper surface of the bedrock.

The accuracy of the estimated sediment volume is dependent on both the identification of the sediment-bedrock interface on the radar transects and on the accuracy of the contouring method employed in creating the isochore map. A GPR investigation by Collins and Doolittle (1989) of similar terrain found the accuracy of the GPR determined depth to bedrock to be within 6 cm, on average, of the actual depth to bedrock as determined by trenching. This suggests that the majority of uncertainty in the sediment overburden volume at GLEES lies in the interpretation and pick of the interface between sediment overburden and bedrock in areas with gradational or non-distinct interface between the two units. Considering that sediment-bedrock interface picks may

vary by ± 0.25 m the possible range of sediment volume at the study site is approximately 90% to 110% of the nominal volume estimated in section 5, suggesting a range from 75,400 to 92,200 m³.

Although the sediment overburden thickness averages 2.5 m and exceeds 9 m near East Glacier Lake, the specific yield estimated for the sediment overburden at the study site is based on representative soil pedon classifications that were completed to only one meter depth (Hopper and Walthall, 1992). In addition, the grain size analyses completed on these soil pedon samples was done only for material that was smaller than 2 mm. Quartzite cobbles and boulders are a large component of the sediment overburden at the study site and therefore must have some effect on specific yield. In a poorly sorted soil quartzite cobbles and boulders take up pore space in the soil and therefore may decrease specific yield. However, if well sorted pockets of quartzite cobbles and boulders exist, an increase in specific yield may result from an increase in interstitial void space. Generally specific yield is considered to decrease with depth as a result of increasing compaction (Johnson, 1967). However, the soil pedons classified at this site appear to generally coarsen with depth, potentially offsetting this effect. All qualitative speculation aside, without direct physical analysis of the sediment overburden at depth it is impossible to quantify the error associated with the specific yield estimate.

The assumption that the study site can be considered representative of the watershed as a whole is based on limited field investigation conducted here and the soil map of Hopper and Walthall (Figure 3) (1992). The GPR investigation indicates that the sediment is generally between 0 and > 4 m thick in the study site, but thickens abruptly to > 9 m in close proximity to East Glacier Lake. The thick section of sediment, proximal

to the lake, may be unique to the geomorphology of the lake. However, a seemingly irregular > 5 m thick sediment pocket located on the divide between East and West Glacier Lakes (Figure 10) suggests that other pockets of thick sediment may be present throughout the watershed as well. The soil types comprising the watershed as a whole, as determined by Hopper and Walthal (1992), are similar to those within the study site with a slightly higher talus component. The sediment overburden volume within the study site may over-represent the sediment overburden volume of the watershed due to the thick section of sediment associated with East Glacier Lake, but the larger component of talus in the upper portion of the watershed with its correspondingly higher specific yield value may offset this effect. Consequently it is difficult to quantify the error introduced in the process of scaling the study site up to the scale of the watershed.

7. Discussion

Outcrops of bedrock provide a tie with radar data (transects T1, T2, and T8) and allow confident determination of the bedrock radar facies signature used to map the interface between sediment overburden and bedrock in the subsurface. The non-distinct interface between sediment overburden and bedrock imaged at depth in many of the radar transects is consistent with the previous seismic refraction survey (Hasfurther et al., 1992). This could indicate that areas of gradation between solid bedrock and sediment overburden (i.e. irregularly weathered bedrock surface) are prevalent at GLEES whereas, areas with distinct boundary between sediment overburden and competent bedrock are the exception. However, as Sass (2006) noted in a similar GPR investigation of alpine talus slope deposits, the non-distinct interface may also result from a lack of dielectric contrast between the sediment overburden and the bedrock. It is assumed that some

combination of these two reasons account for the non-distinct interface between sediment overburden and bedrock at depth seen in the radar data at GLEES.

The water table was not imaged during this survey, or if it was, the contrast between it and reflections from other subsurface heterogeneities was indistinguishable. Therefore, the attempt to correlate an imaged water table in the radar data with the water level in East Glacier Lake was unsuccessful. The average radar wave velocity of 0.06 m/ns determined in this study is considered slow for radar waves travelling through dry materials (Table 1), even including clays, which are not a dominant component of the sediment at this site. However, this velocity is comparable to that of radar traveling through saturated sand and gravel or saturated silt (Davis and Annan, 1989; Neal, 2004; Leopold et al., 2008). This survey was completed in the late summer/early fall after snowmelt from a relatively large snowpack year. The outlet stream of East Glacier Lake was still running, indicating that groundwater input to the lake had not yet ceased. Under these conditions a saturated subsurface is not unlikely in portions of the study site and semi-saturated conditions may be prevalent as indicated by the observed low radar velocity. The water table would therefore be very near to the surface and potentially obscured by the direct air and ground radar waves. Another possible reason for non-detection of the water table is that the water table may not be a sharp interface, but a gradational one (Annan et al., 1991). Due to capillary action this gradational zone may be very broad in fine grained materials such as the soils classified by Hopper and Walthall (1992).

The bedrock fracture density of only 1 fracture per 4,810 m² is surprising considering the frequency of fracturing evident in bedrock outcrop at GLEES. However,

considering the 100 MHz GPR resolution of approximately 0.25 m the fractures imaged in the radar data are large scale fractures. There may be many more fractures at a smaller scale that are too fine for the 100 MHz GPR to resolve. Also, a bedrock fracture may not produce a radar signature if there is not a contrast in dielectric permittivity between the bedrock and the substance filling the fracture.

Fractures F2, F3 and F6 seem to propagate into the sediment overburden. A potential explanation for this is that the bedrock fracture developed or has continued to grow post deposition of the sediment overburden in response to unloading of material removed by the last glaciation. Another possibility is that what has been considered sediment overburden from the radar facies analysis is in fact a zone of highly weathered and fractured bedrock in which the bedrock fracture is still intact.

The bedrock surface contour map developed in this study (Figure 13) suggests no groundwater connection between East and West Glacier Lakes through the sediment overburden (the bedrock ridge between the two lakes forms a hydrologic barrier). However, the presence of large bedrock fractures suggests that there is potential for a fractured bedrock aquifer that may link the two lakes. A higher resolution survey over a denser survey grid is required to either confirm or deny the existence of such a fractured bedrock aquifer. The area around the East Glacier Lake flume gauge contains sediment thickness of up to > 4 m which potentially allows groundwater to bypass the flume gauge. The hypolon liner installed at this location may not be adequate to capture all flow leaving the watershed.

8. Conclusions

A ground penetrating radar (GPR) survey was conducted in the Snowy Range of Wyoming at the Glacier Lakes Ecosystem Experiment Site (GLEES) to assess the potential of groundwater storage. The site is located at approximately 3,300 m amsl in an alpine to subalpine ecological zone. The subsurface geology at the study site is quartzite bedrock overlain by poorly sorted unconsolidated sediments comprised of quartzite boulders and cobbles and poorly developed soils. A Sensors and Software® PulseEKKO® 100 GPR system with 100 MHz antennas was used to collect radar data of the subsurface along 12 transects around East Glacier Lake. The data were analyzed to determine the thickness of sediment overburden at the site and the density of bedrock fractures. A radar facies analysis was used to distinguish sediment overburden from the quartzite bedrock. Bedrock outcrops were identified and included in the survey transects to correlate with the bedrock radar facies in the subsurface.

Sediment overburden thickness ranges from 0 m at bedrock outcrops to > 9 m near East Glacier Lake. The volume of sediment at the study site is $83,800 \pm 8,380 \text{ m}^3$. Average specific yield for the study site is approximately 10%, therefore the maximum potential change in groundwater storage is $8,380 \pm 838 \text{ m}^3$ for the study site. Considering that the area of the study site is only 12% of the East Glacier Lake watershed as a whole, this corresponds to $61,300 \pm 6,130 \text{ m}^3$ of maximum potential change in groundwater storage at the East Glacier Lake watershed scale. A change of this magnitude is equal to approximately 17% of the average annual precipitation ($356,000 \text{ m}^3$), and approximately 24% of the average annual surface water discharge ($258,000 \text{ m}^3$) recorded for the East Glacier Lake watershed. Any contribution to groundwater storage from a fractured bedrock aquifer would be in addition to this.

The estimated annual groundwater discharge in the area of the outlet stream is approximately 3,140 m³ based on the average saturated hydraulic conductivity of the sediment aquifer determined by Houghton et al. (2011), the hydraulic gradient as determined between the water level of East Glacier Lake at the outlet stream and the ground elevation at the intersection of transects T4b and L2, and the cross sectional area of the sediment aquifer at transect T4b.

9. Recommendations for Future Study

The ability to tie geophysical data to points of direct observation at depth, such as borehole log data, is required to minimize uncertainty in geophysical interpretations of the subsurface. Ideally, an arrangement could be made with the USDA Forest Service to permit a borehole investigation at GLEES to tie to the results of the GPR investigation. Completion of groundwater monitoring wells in three or more boreholes could provide data to more accurately determine saturated hydraulic conductivity and hydraulic gradient in the unconfined sediment overburden aquifer and possibly in the bedrock, depending on the depth of completion.

Considering the unlikelihood of such an arrangement with the Forest Service and the high cost associated with a borehole investigation in a road-less area, the second best recommendation for future work is to perform additional geophysical investigations using a variety of geophysical methods (i.e. electrical resistivity and seismic refraction). The benefit of conducting additional geophysical investigations at GLEES is the low-cost, portable, non-invasive nature of geophysical surveys and the ability to compare results from each geophysical method to compile the best composite interpretation of the subsurface available without a direct physical investigation. In addition, temporally

spaced geophysical surveys throughout a field season may provide insight into the seasonal change in groundwater storage if it is possible to identify and monitor changing levels of the water table through time or to infer changes in moisture content.

10. References

- Annan, A.P., Cosway, S.W. and Redman, J.D. 1991. Water table detection with ground-penetrating radar. *Expanded Abstracts 61st Annual International Meeting of the Society of Exploration Geophysicists*, 494 – 496. Society of Exploration Geophysicists.
- Beres Jr. M., Haeni, F.P. 1991. Application of ground-penetrating-radar methods in hydrogeologic studies. *Ground Water*, 29, 375 – 386.
- Berthling, I., Etzelmuller, B., Isaksen, K. and Sollid, J.L. 2000. Rock glaciers on Prins Karls Forland. II: GPR soundings and the development of internal structures. *Permafrost and Periglacial Processes*, 11, 357 – 369.
- Collins, M.E., Doolittle, J.A. and Rourke, R.V. 1989. Mapping depth to bedrock on a glaciated landscape with ground-penetrating radar. *Soil Science Society of America Journal*, 53, 1806 – 1812.
- Davis, J.L. and Annan, A.P. 1989. Ground-penetrating radar for high-resolution mapping of soil and rock stratigraphy. *Geophysical Prospecting*, 37, 531 – 551.
- Degenhardt Jr., J.J., Giardino, J.R. and Junck, B. 2003. GPR survey of a lobate rock glacier in Yankee Boy Basin, Colorado, USA. In: *Ground Penetrating Radar in Sediments* (C.S. Bristow and H.M. Jol, eds), 167 – 179. Geological Society, London, Special Publications 211.
- Ekes, C. and Hickin, E.J. 2001. Ground penetrating radar radices of the paraglacial Cheekye Fan, southwestern British Columbia, Canada. *Sedimentary Geology*, 143, 199 – 217.
- Garmin. 2003. *eTrex Personal Navigator Owner's Manual*. Garmin International, Incorporated, 52 pp.
- Hasfurther VC, Kerr GL, Parks G and Wetstein J. 1992. Chapter 9 “Hydrology” in *The Glacier Lakes Ecosystem Experiments Site*, R.C. Musselman (editor), General Technical Report RM-249, 50 – 56.
- Hopper, R.W.E. and Walthall, P.M. 1992. Chapter 5 “Soils” in *The Glacier Lakes Ecosystem Experiments Site*, R.C. Musselman (editor), General Technical Report RM-249, 23 – 29.
- Houghton, T.H., M.J. Ronayne, and J.D. Stednick. 2011. Dependence of hydraulic conductivity on measurement scale in an alpine glacial till, AGU Hydrology Days 2011, Fort Collins, Colorado.

- Hultstrand, D.M., 2006. Geostatistical methods for estimating snowmelt contribution to an alpine water balance. M.S. Thesis, Department of Earth Resources, Colorado State University. 117 pp.
- Johnson, A.I. 1967. Specific yield – compilation of specific yields for various materials. U.S. Geological Survey Water Supply Paper 1662-D. 74 pp.
- Jol, H.M. and Smith, D.G. 1991. Ground penetrating radar of northern lacustrine deltas. *Canadian Journal of Earth Sciences* 28, 1939 – 1947.
- Leopold, M., Dethier, D., Volkel, J., Raab, T., Rikert, T.C. and Caine, N. 2008. Using Geophysical Methods to Study the Shallow Subsurface of a Sensitive Alpine Environment, Niwot Ridge, Colorado Front Range, U.S.A. *Arctic, Antarctic, and Alpine Research*, 40, 519 – 530. DOI: 10.1657/1523-0430(06-124)[LEOPOLD]2.0.CO;2
- Musselman, R.C., Fox, D.G., Schoettle, A.W. and Regan, C.M. 1992. Chapter 1 “Introduction” in *The Glacier Lakes Ecosystem Experiments Site*, R.C. Musselman (editor), General Technical Report RM-249, 1 – 10.
- Monnier, S., Camerlynck, C. and Rejiba, F. 2008. Ground penetrating radar survey and stratigraphic interpretation of the Plan du Lac Rock Glaciers, Vanoise Massif, Northern French Alps. *Permafrost and Periglacial Processes*, 19, 19 – 30. doi:10.1002/ppp.610
- Neal, A. 2004. Ground-penetrating radar and its use in sedimentology: principals, problems and progress. *Earth-Science Reviews*, 66, 261 – 330. doi:10.1016/j.earscirev.2004.01.004
- Rochette, E.A. 1992. Chapter 4 “Geology” in *The Glacier Lakes Ecosystem Experiments Site*, R.C. Musselman (editor), General Technical Report RM-249, 20 – 22.
- Sass, O. 2006. Determination of the internal structure of alpine talus deposits using different geophysical methods (Lechtaler Alps, Austria). *Geomorphology*, 80, 45 – 58. doi:10.1016/j.geomorph.2005.09.006
- Sensors and Software. 1999. *PulseEKKO 100 RUN User’s Guide, Version 1.2*. Sensors and Software, Ontario, 77 pp.
- Sensors and Software. 2003. *EKKO_View Enhanced and EKKO_View Deluxe User’s Guide*. Sensors and Software, Ontario, 132 pp.
- Schwartz, F.W. and Zhang, H. 2003. *Fundamentals of Groundwater*. John Wiley & Sons, New York, 592 pp.
- Tearpock, D.J. and Bischke, R.E. 2003. *Applied Subsurface Geological Mapping With Structural Methods*, 2nd edn. Prentice Hall PTR, New Jersey, 822 pp.

van Overmeeren, R.A. 1998. Radar facies of unconsolidated sediments in The Netherlands: A radar stratigraphy interpretation method for hydrogeology. *Journal of Applied Geophysics*, 40, 1 – 18.

Vertucci, F.A. and Conrad, M.A. 1992. Chapter 6 “*Aquatics*” in *The Glacier Lakes Ecosystem Experiments Site*, R.C. Musselman (editor), General Technical Report RM-249, 30 – 41.

Appendix A: GPR Transects

List of Figures

Figure A1 - a) GPR transect L1. Elevation is relative to the water level of East Glacier Lake (3,282m amsl). Depths below ground level are based on an average radar velocity of 0.06 m/ns. b) Interpreted GPR transect L1. A bedrock fracture (F1) centered at approximately 75m is shown in red.....	50
Figure A2 - a) GPR transect L2. Elevation is relative to the water level of East Glacier Lake (3,282m amsl). Depths below ground level are based on an average radar velocity of 0.06 m/ns. b) Interpreted GPR transect L2. A bedrock fracture (F2) centered at approximately 72m is shown in red.....	52
Figure A3 - a) GPR transect L3. Elevation is relative to the water level of East Glacier Lake (3,282m amsl). Depths below ground level are based on an average radar velocity of 0.06 m/ns. b) Interpreted GPR transect L3.....	54
Figure A4 - a) GPR transect T1. Elevation is relative to the water level of East Glacier Lake (3,282m amsl). Depths below ground level are based on an average radar velocity of 0.06 m/ns. b) Interpreted GPR transect T1.....	56
Figure A5 - a) GPR transect T2. Elevation is relative to the water level of East Glacier Lake (3,282m amsl). Depths below ground level are based on an average radar velocity of 0.06 m/ns. b) Interpreted GPR transect T2. A bedrock fracture (F1) centered at approximately 42m is shown in red.....	58
Figure A6 - a) GPR transect T3. Elevation is relative to the water level of East Glacier Lake (3,282m amsl). Depths below ground level are based on an average radar velocity of 0.06 m/ns. b) Interpreted GPR transect T3.....	60
Figure A7 - a) GPR transect T4a. Elevation is relative to the water level of East Glacier Lake (3,282m amsl). Depths below ground level are based on an average radar velocity of 0.06 m/ns. b) Interpreted GPR transect T4a. A bedrock fracture (F4) centered at approximately 60m is shown in red.....	62
Figure A8 - a) GPR transect T4b. Elevation is relative to the water level of East Glacier Lake (3,282m amsl). Depths below ground level are based on an average radar velocity of 0.06 m/ns. b) Interpreted GPR transect T4b.....	64

Figure A9 - a) GPR transect T5. Elevation is relative to the water level of East Glacier Lake (3,282m amsl). Depths below ground level are based on an average radar velocity of 0.06 m/ns. b) Interpreted GPR transect T5. A bedrock fracture (F3) centered at approximately 13m is shown in red..... 66

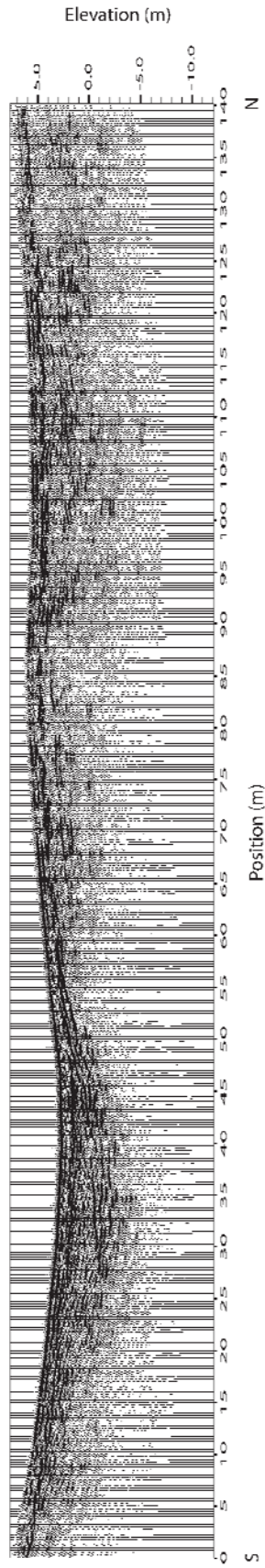
Figure A10 - a) GPR transect T6. Elevation is relative to the water level of East Glacier Lake (3,282m amsl). Depths below ground level are based on an average radar velocity of 0.06 m/ns. b) Interpreted GPR transect T6. A bedrock fracture (F2) centered at approximately 24m is shown in red..... 68

Figure A11 - a) GPR transect T7. Elevation is relative to the water level of East Glacier Lake (3,282m amsl). Depths below ground level are based on an average radar velocity of 0.06 m/ns. b) Interpreted GPR transect T7..... 70

Figure A12 - a) GPR transect T8. Elevation is relative to the water level of East Glacier Lake (3,282m amsl). Depths below ground level are based on an average radar velocity of 0.06 m/ns. b) Interpreted GPR transect T8. Bedrock fractures (F5, F6, and F7) centered at approximately 6, 46, and 73m respectively are shown in red.. 72

Figure A1 - a) GPR transect L1. Elevation is relative to the water level of East Glacier Lake (3,282m amsl). Depths below ground level are based on an average radar velocity of 0.06 m/ns. b) Interpreted GPR transect L1. A bedrock fracture (F1) centered at approximately 75m is shown in red.

a)



b)

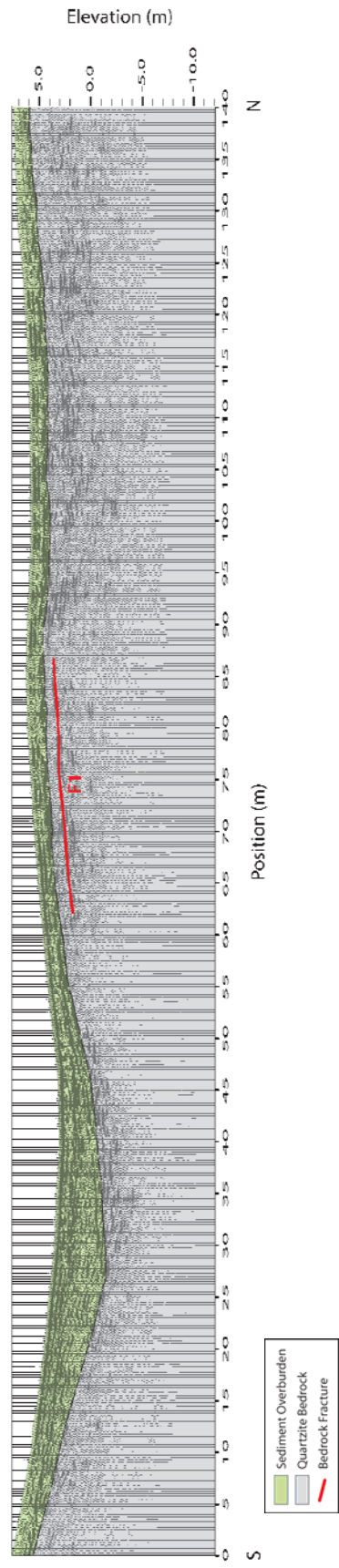
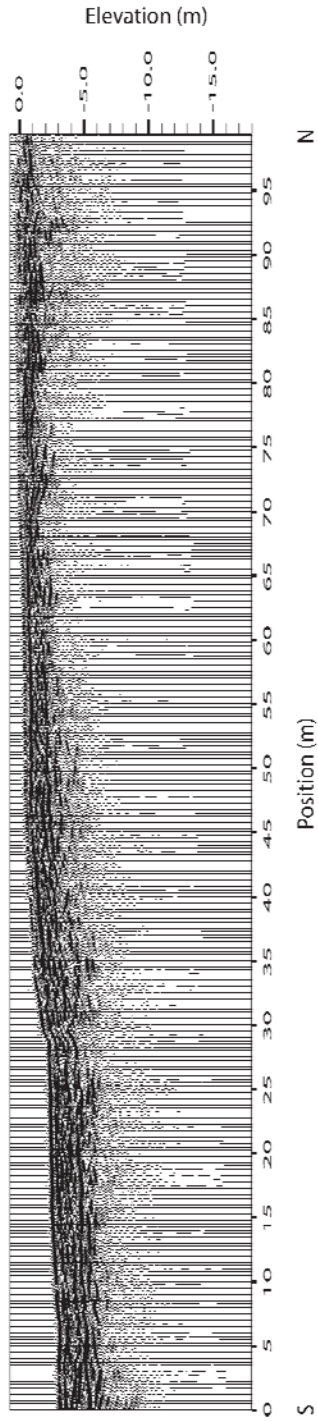


Figure A2 – a) GPR transect L2. Elevation is relative to the water level of East Glacier Lake (3,282m amsl). Depths below ground level are based on an average radar velocity of 0.06 m/ns. b) Interpreted GPR transect L2. A bedrock fracture (F2) centered at approximately 72m is shown in red.

a)



b)

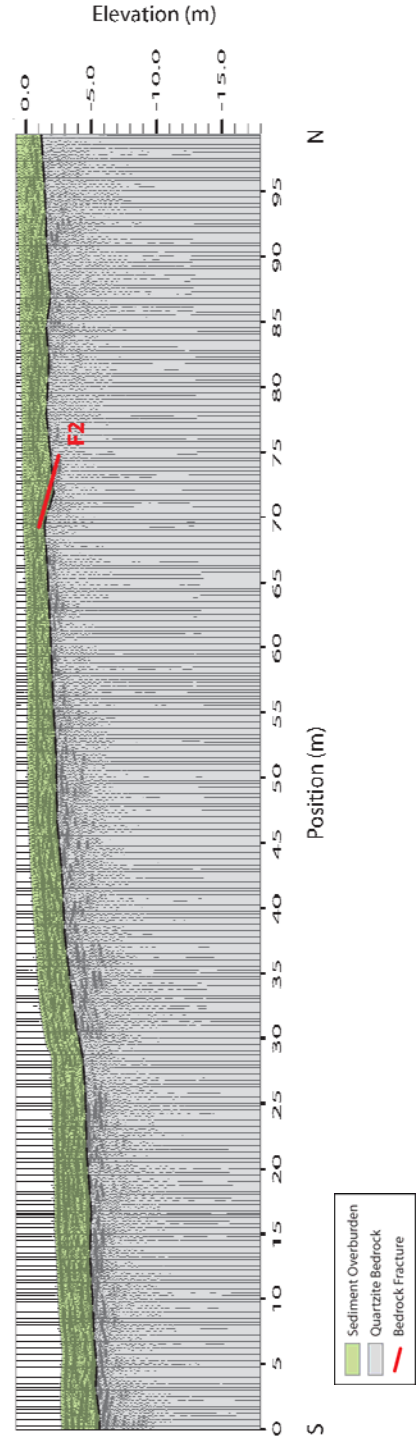


Figure A3 - a) GPR transect L3. Elevation is relative to the water level of East Glacier Lake (3,282m amsl). Depths below ground level are based on an average radar velocity of 0.06 m/ns. b) Interpreted GPR transect L3.

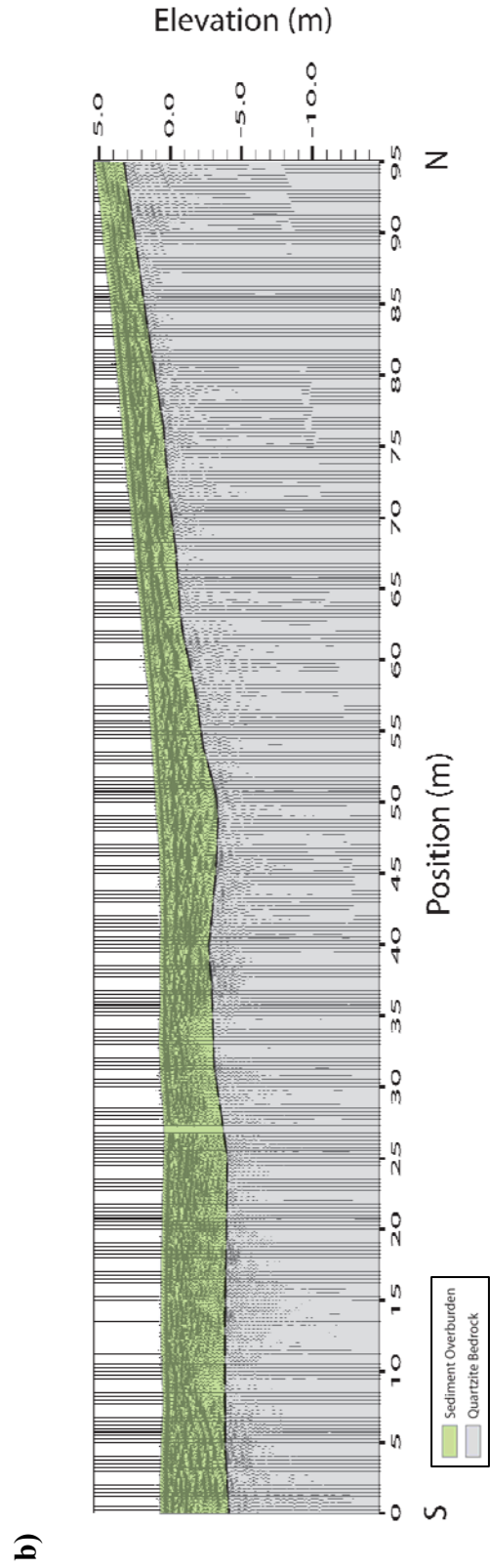
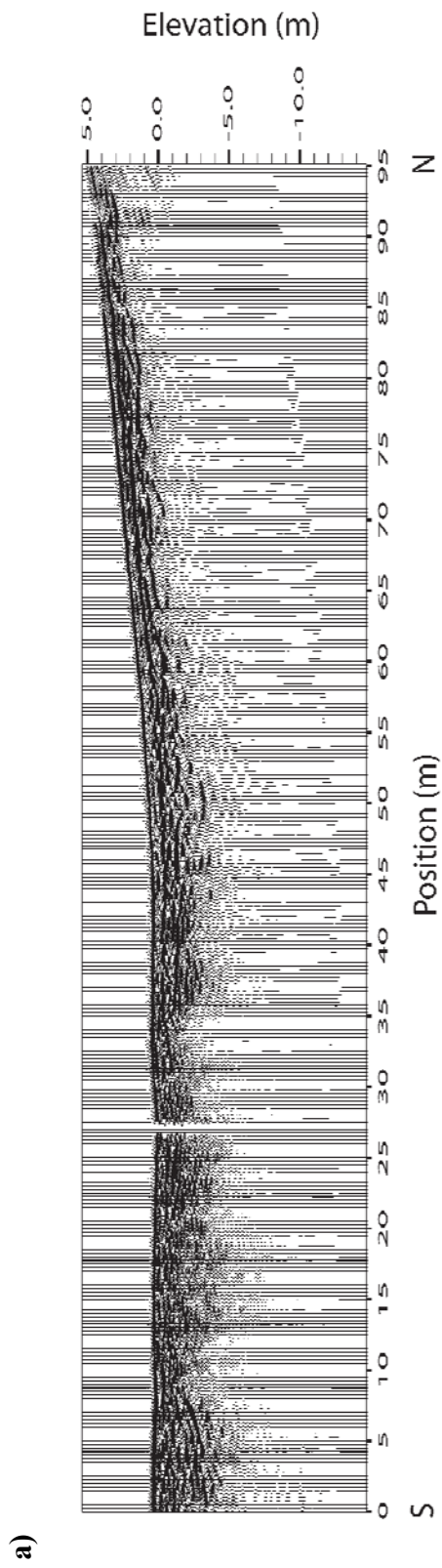


Figure A4 - a) GPR transect T1. Elevation is relative to the water level of East Glacier Lake (3,282m amsl). Depths below ground level are based on an average radar velocity of 0.06 m/ns. b) Interpreted GPR transect T1.

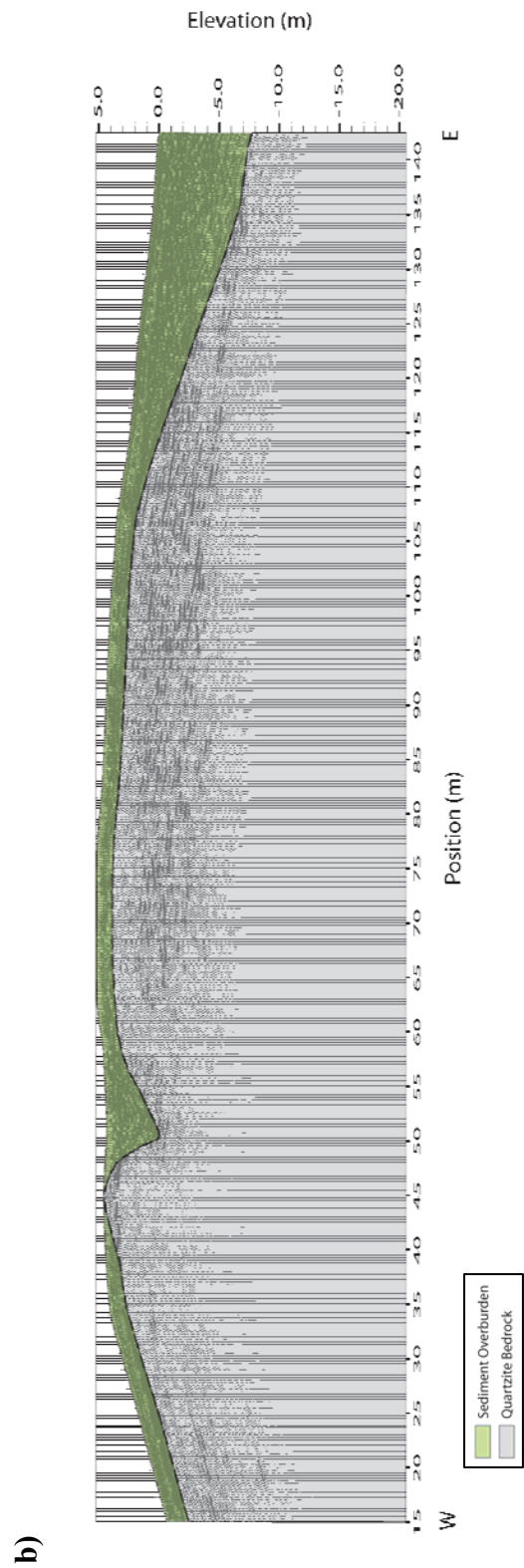
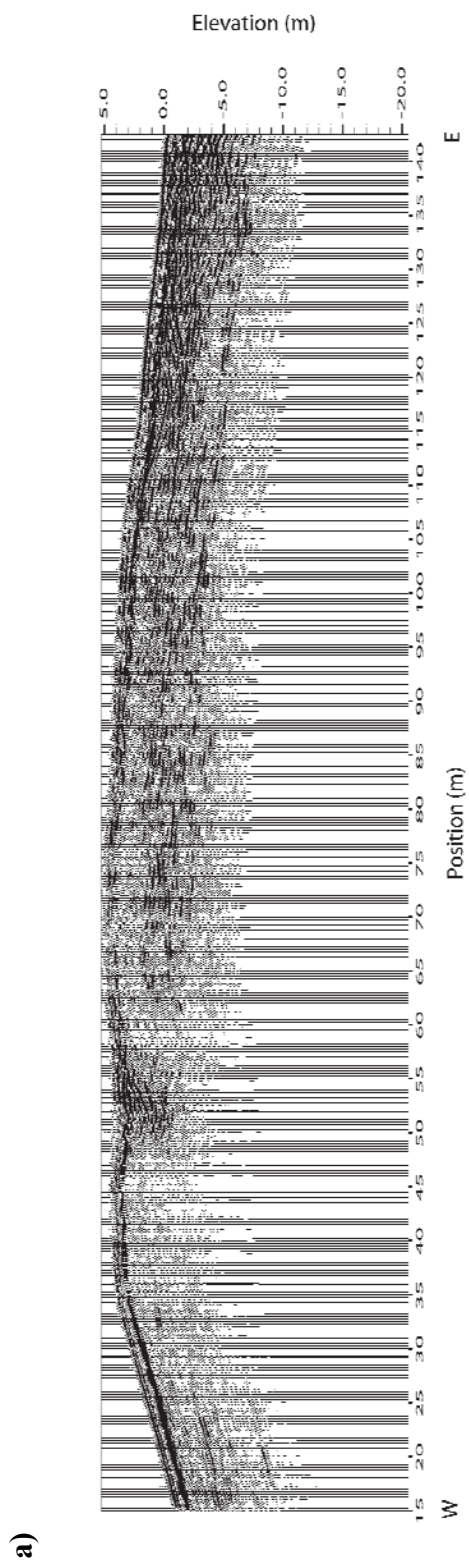


Figure A5 - a) GPR transect T2. Elevation is relative to the water level of East Glacier Lake (3,282m amsl). Depths below ground level are based on an average radar velocity of 0.06 m/ns. b) Interpreted GPR transect T2. A bedrock fracture (F1) centered at approximately 42m is shown in red.

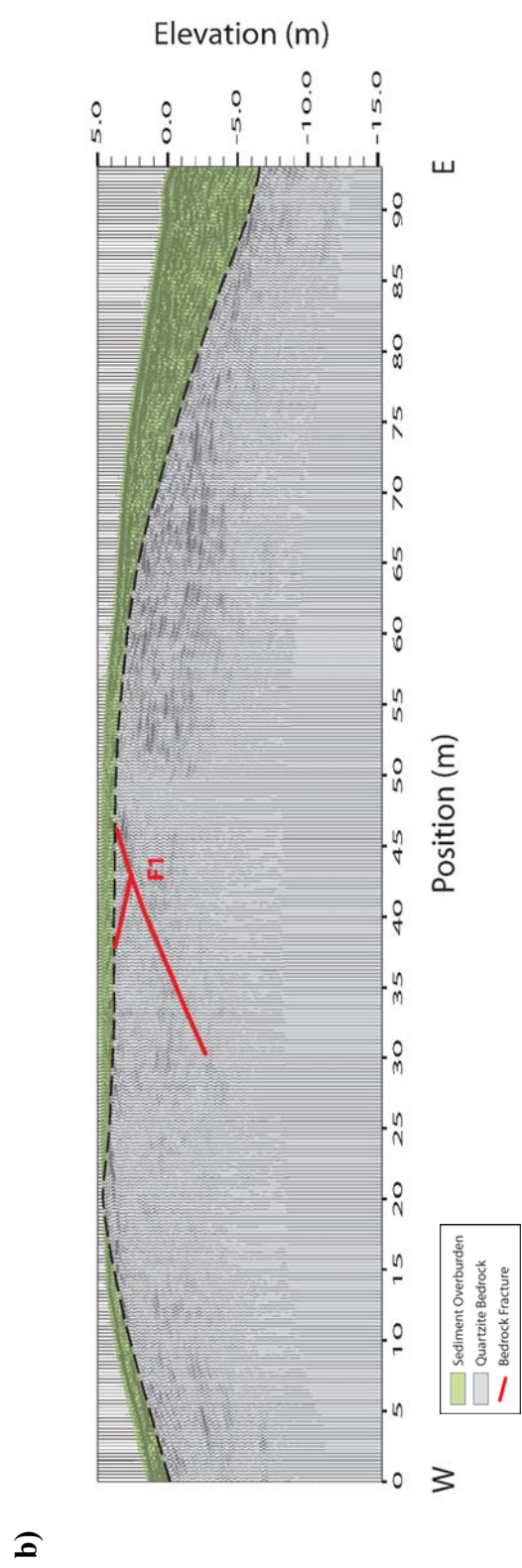
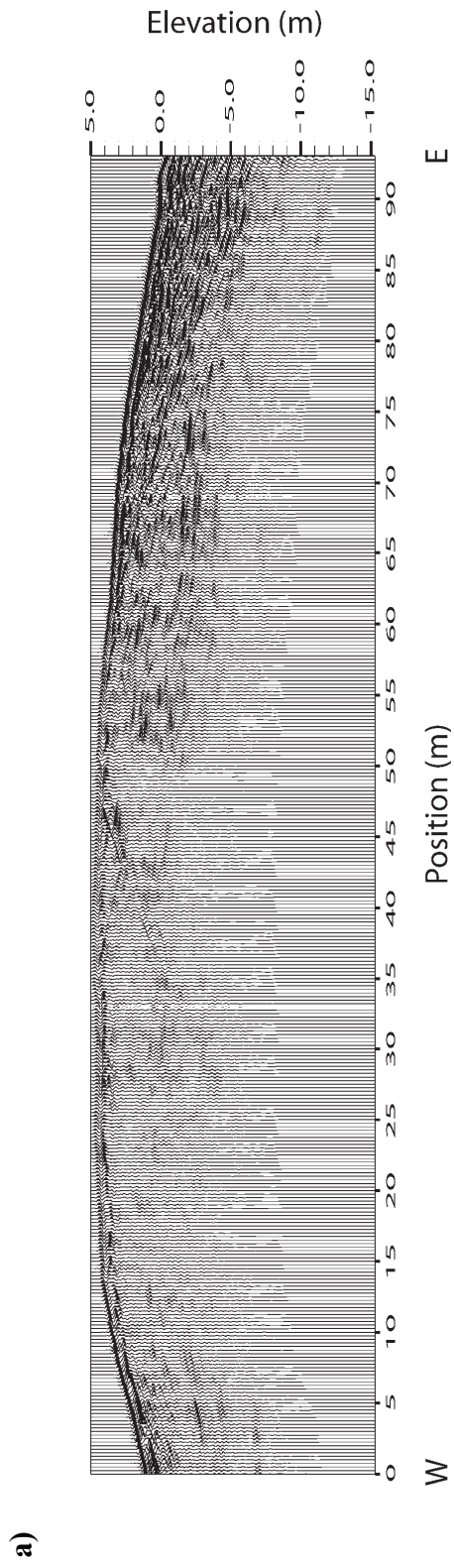
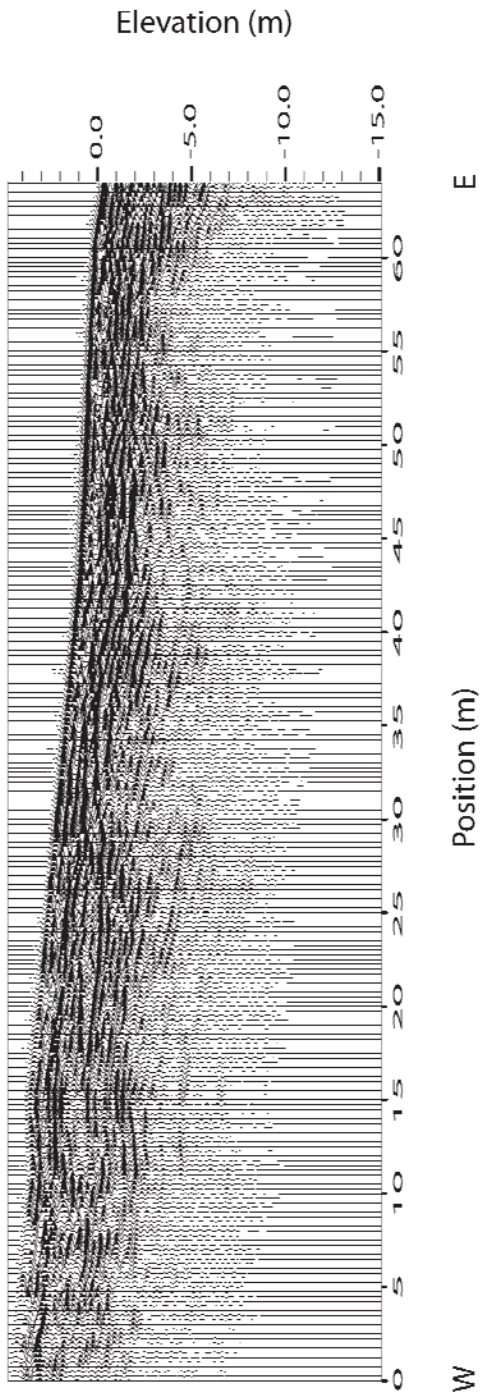


Figure A6 - a) GPR transect T3. Elevation is relative to the water level of East Glacier Lake (3,282m amsl). Depths below ground level are based on an average radar velocity of 0.06 m/ns. b) Interpreted GPR transect T3.

a)



b)

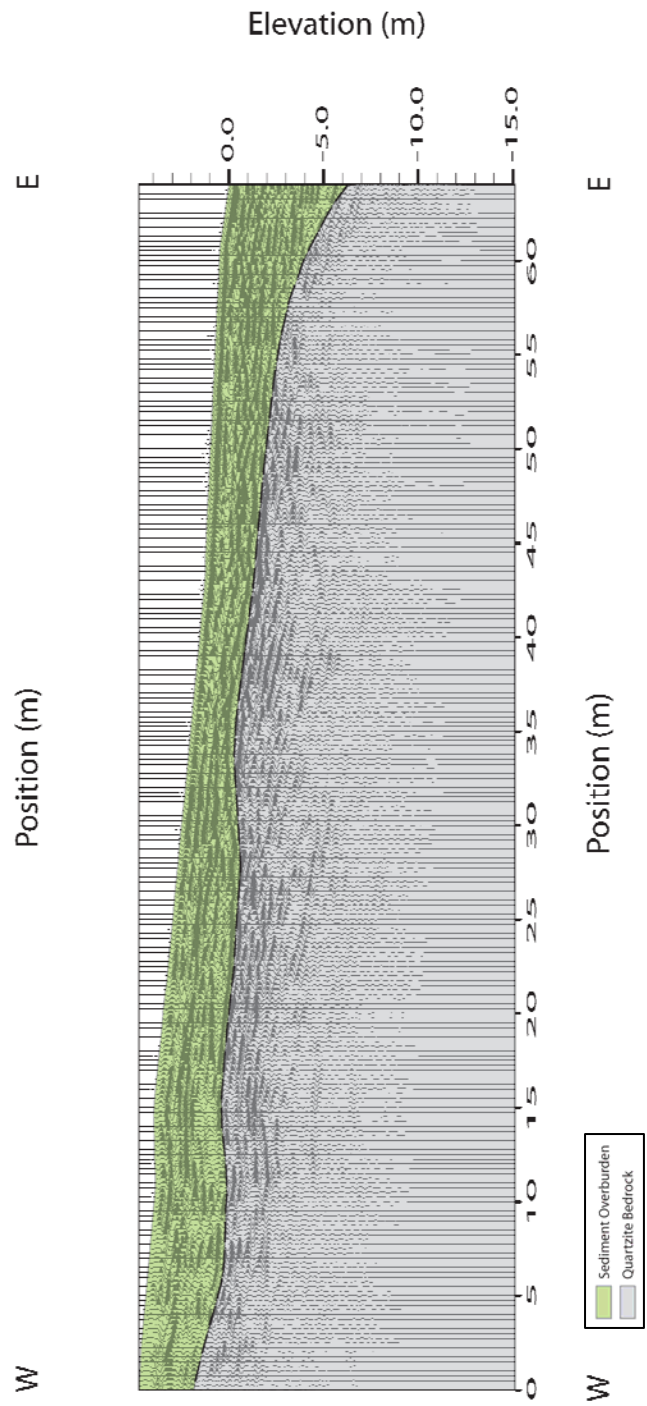
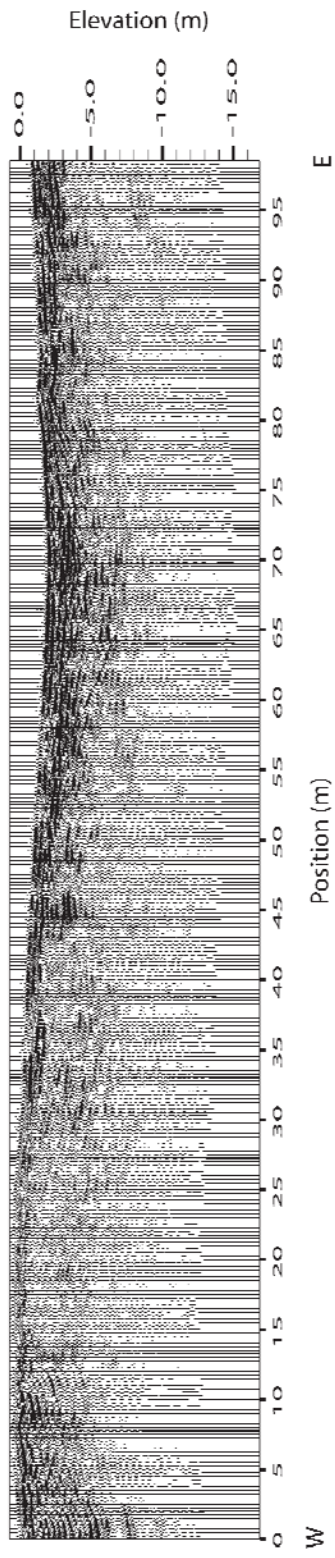


Figure A7 - a) GPR transect T4a. Elevation is relative to the water level of East Glacier Lake (3,282m amsl). Depths below ground level are based on an average radar velocity of 0.06 m/ns. b) Interpreted GPR transect T4a. A bedrock fracture (F4) centered at approximately 60m is shown in red.

a)



b)

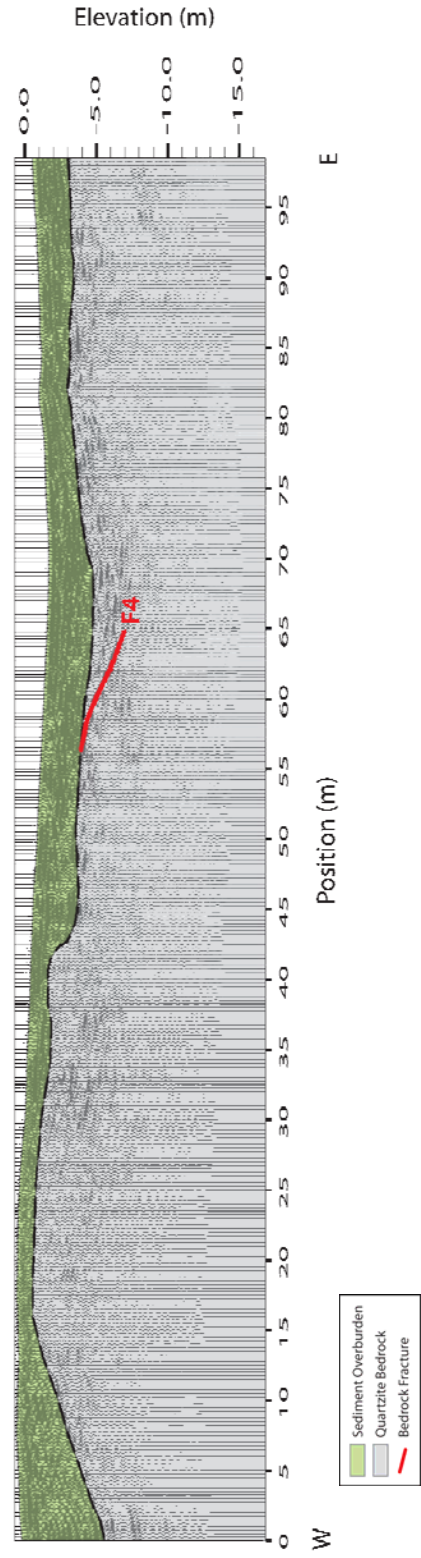
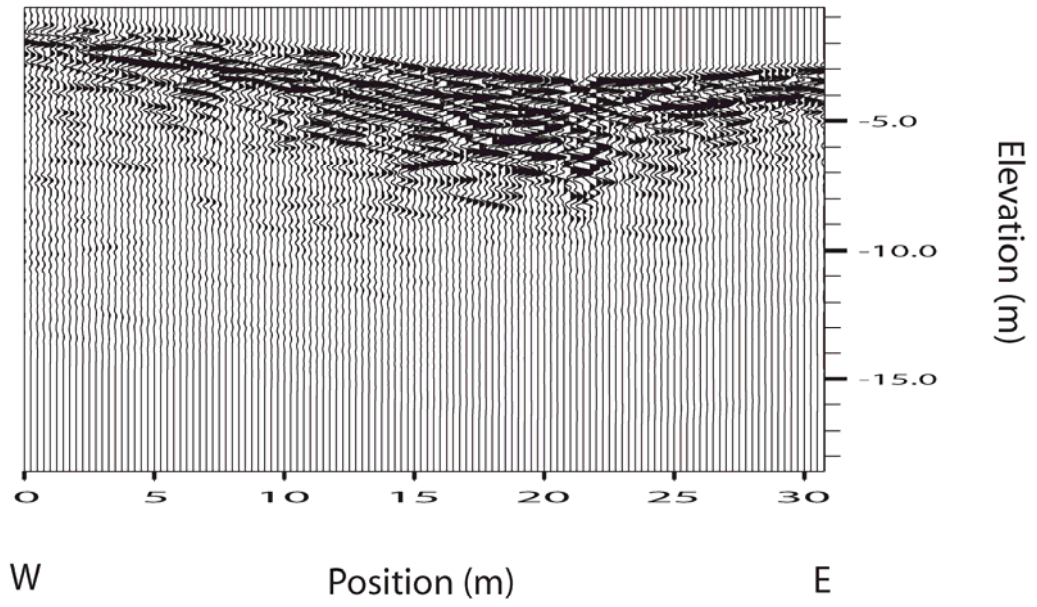


Figure A8 - a) GPR transect T4b. Elevation is relative to the water level of East Glacier Lake (3,282m amsl). Depths below ground level are based on an average radar velocity of 0.06 m/ns. b) Interpreted GPR transect T4b.

a)



b)

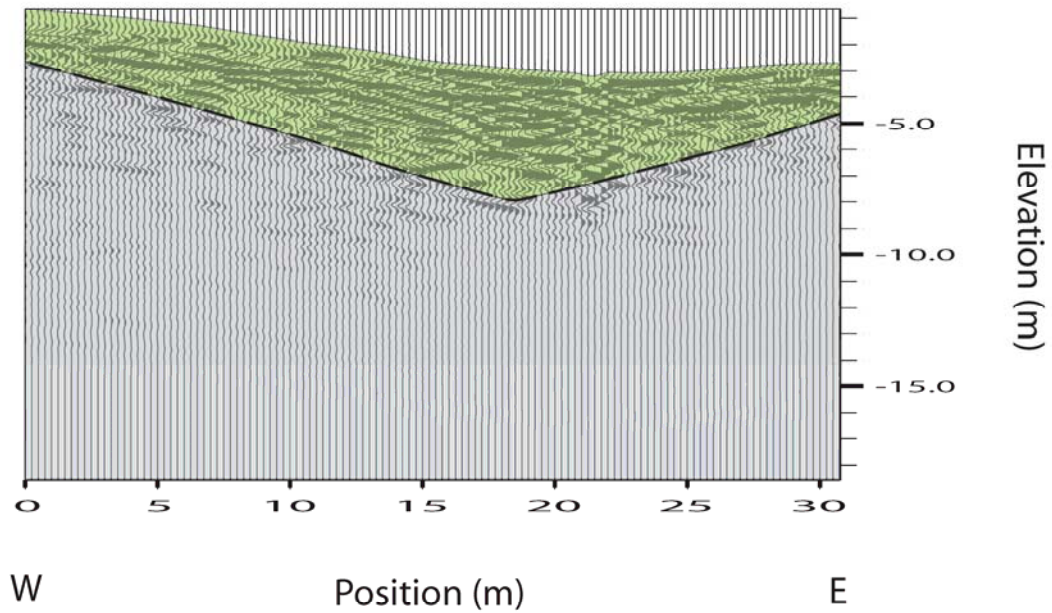


Figure A9 - a) GPR transect T5. Elevation is relative to the water level of East Glacier Lake (3,282m amsl). Depths below ground level are based on an average radar velocity of 0.06 m/ns. b) Interpreted GPR transect T5. A bedrock fracture (F3) centered at approximately 13m is shown in red.

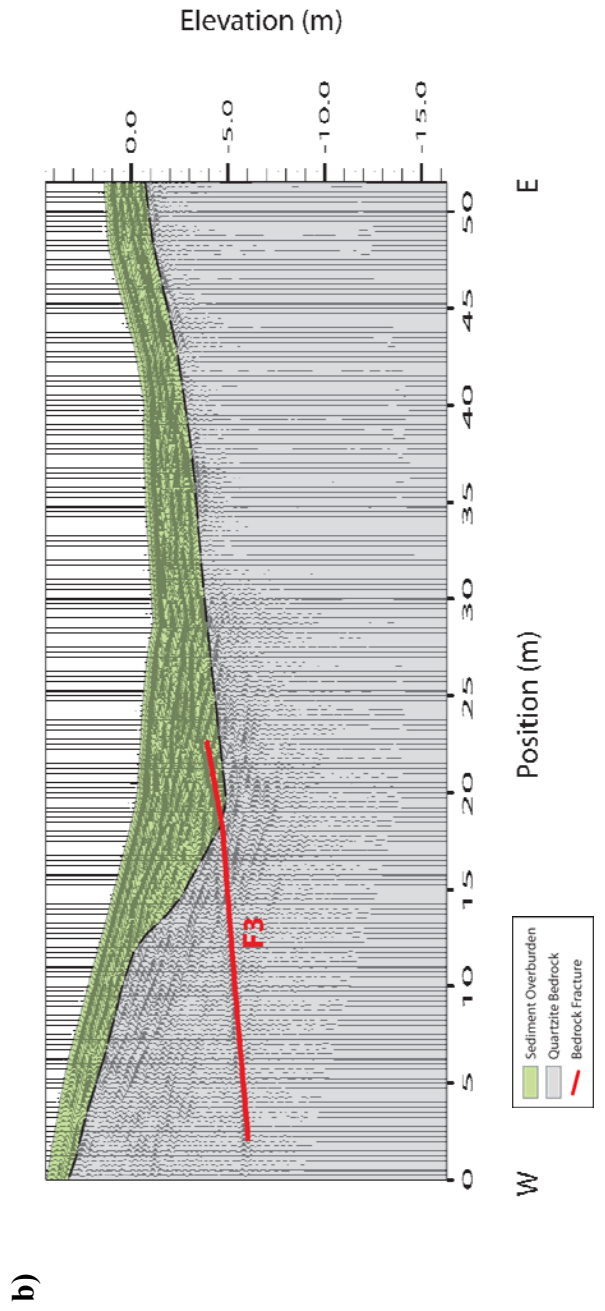
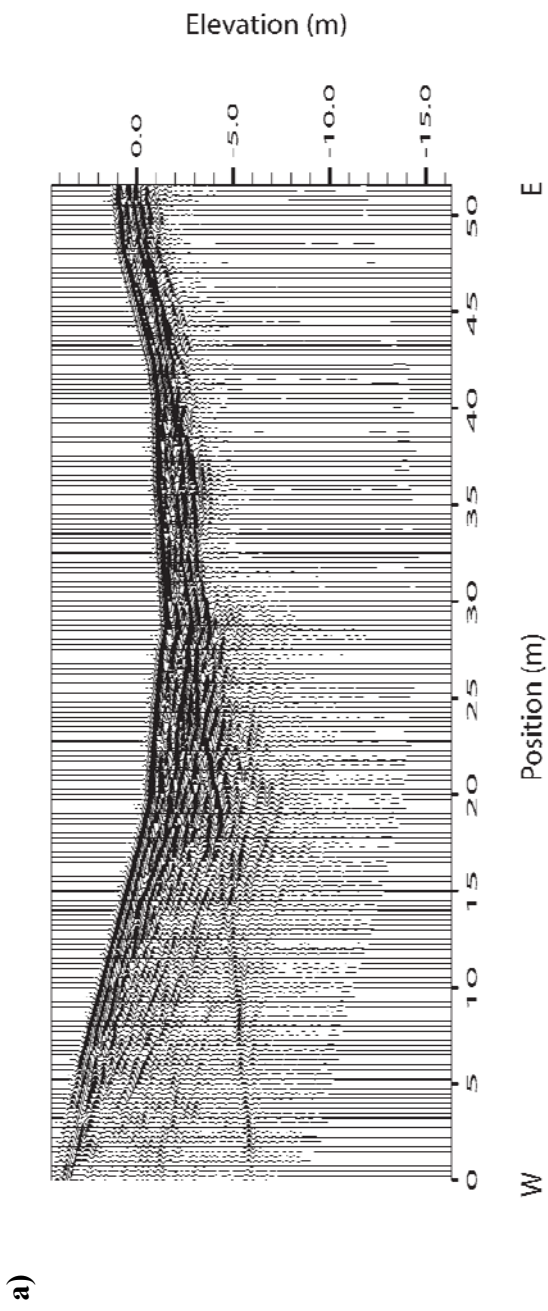


Figure A10 - a) GPR transect T6. Elevation is relative to the water level of East Glacier Lake (3,282m amsl). Depths below ground level are based on an average radar velocity of 0.06 m/ns. b) Interpreted GPR transect T6. A bedrock fracture (F2) centered at approximately 24m is shown in red.

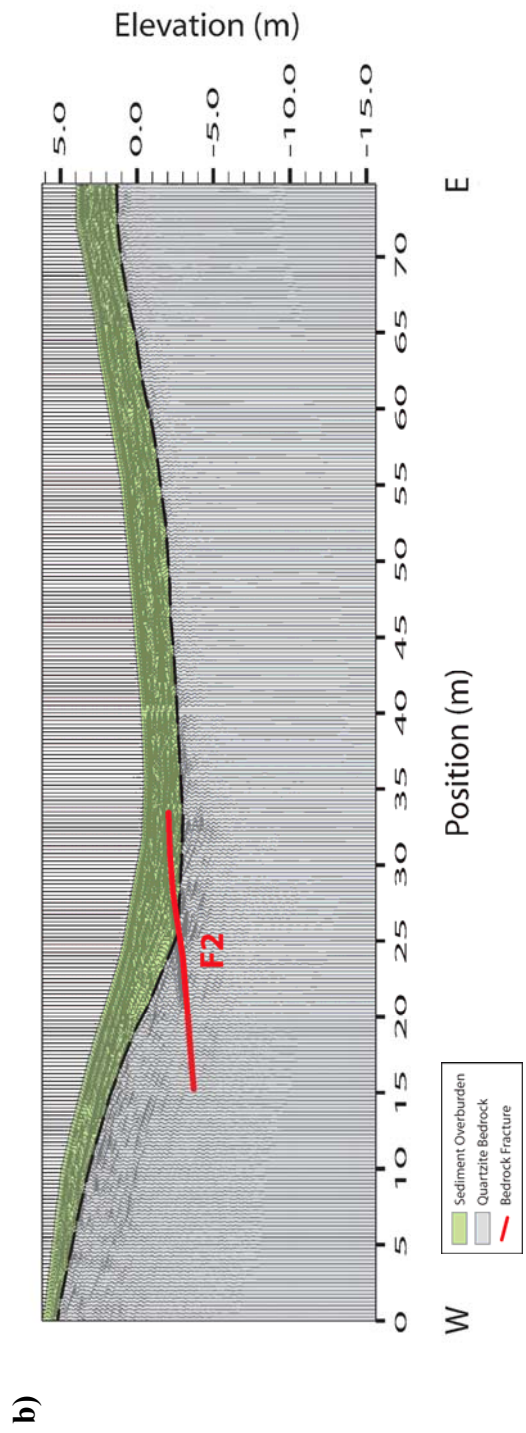
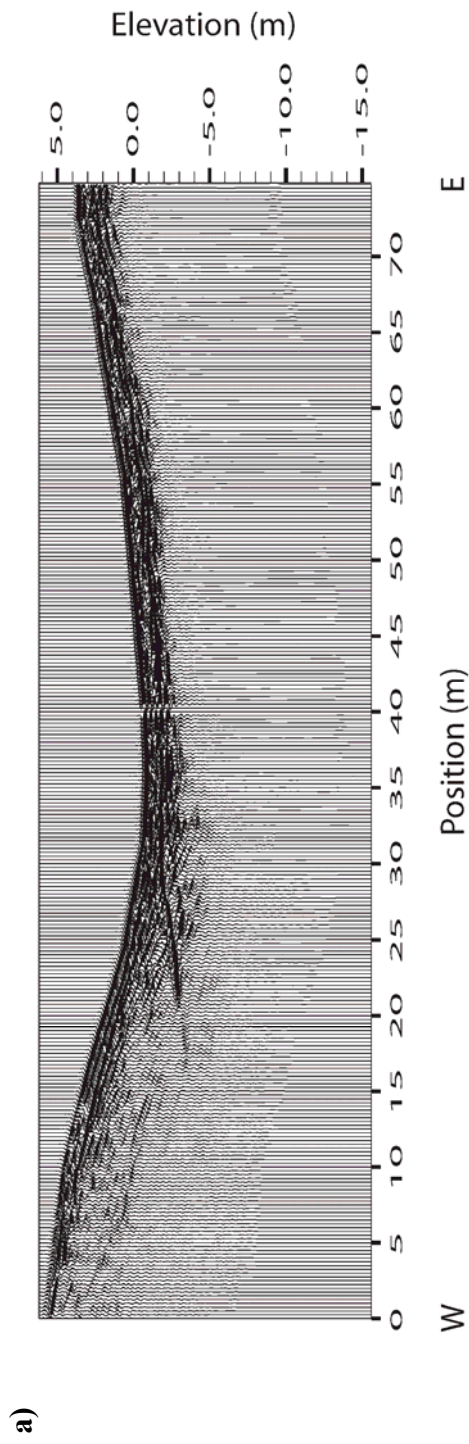


Figure A11 - a) GPR transect T7. Elevation is relative to the water level of East Glacier Lake (3,282m amsl). Depths below ground level are based on an average radar velocity of 0.06 m/ns. b) Interpreted GPR transect T7.

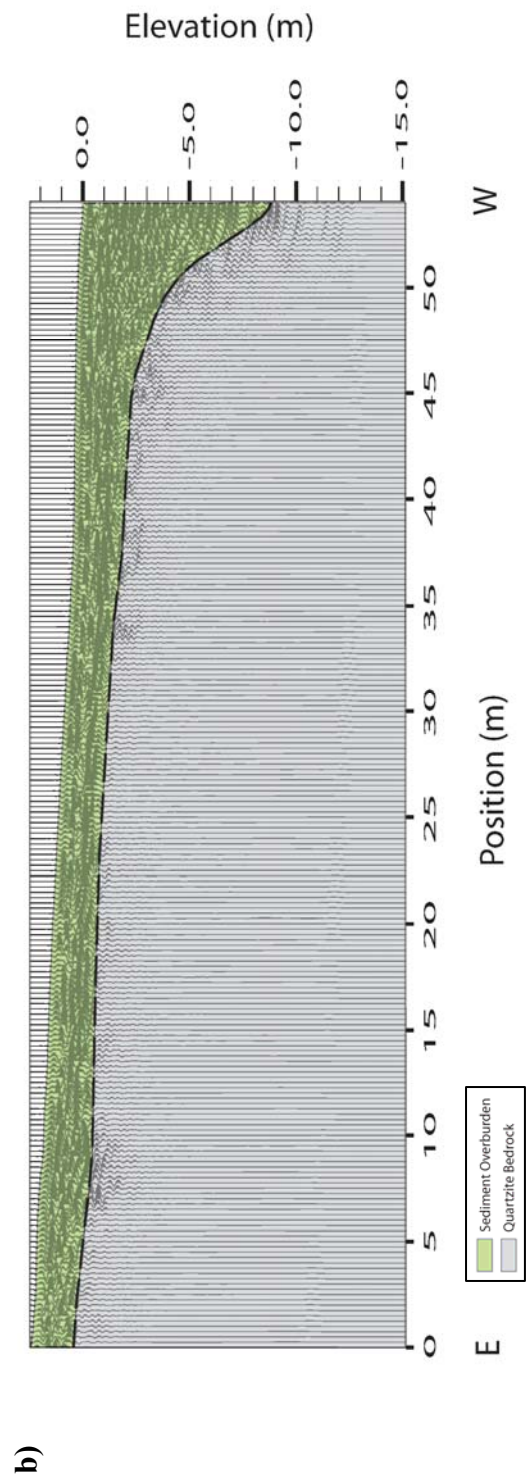
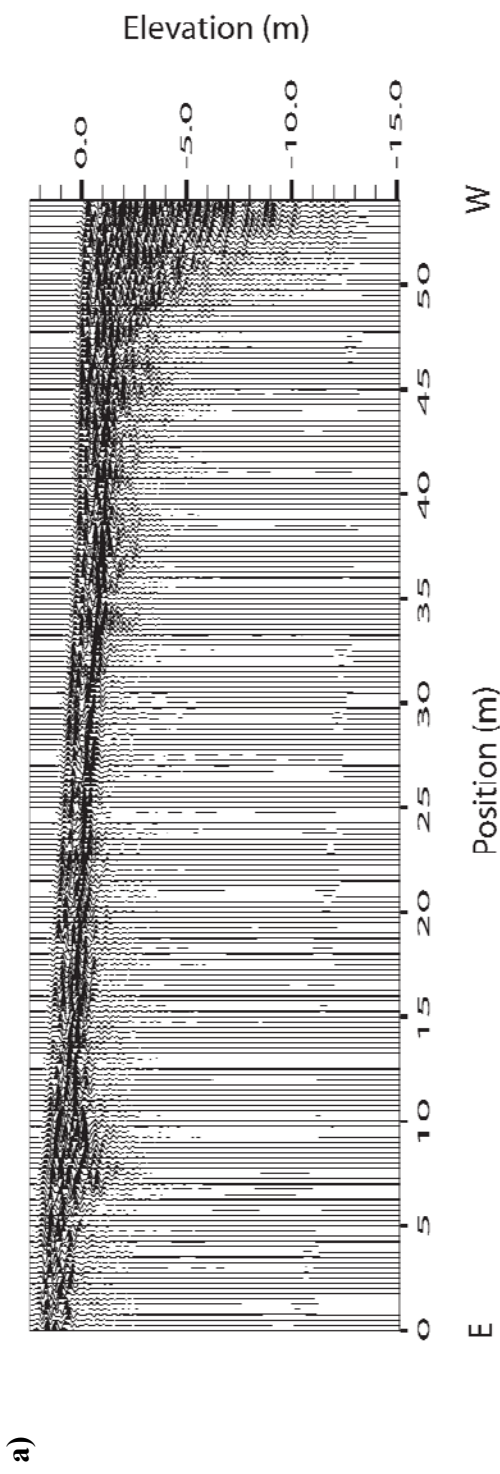
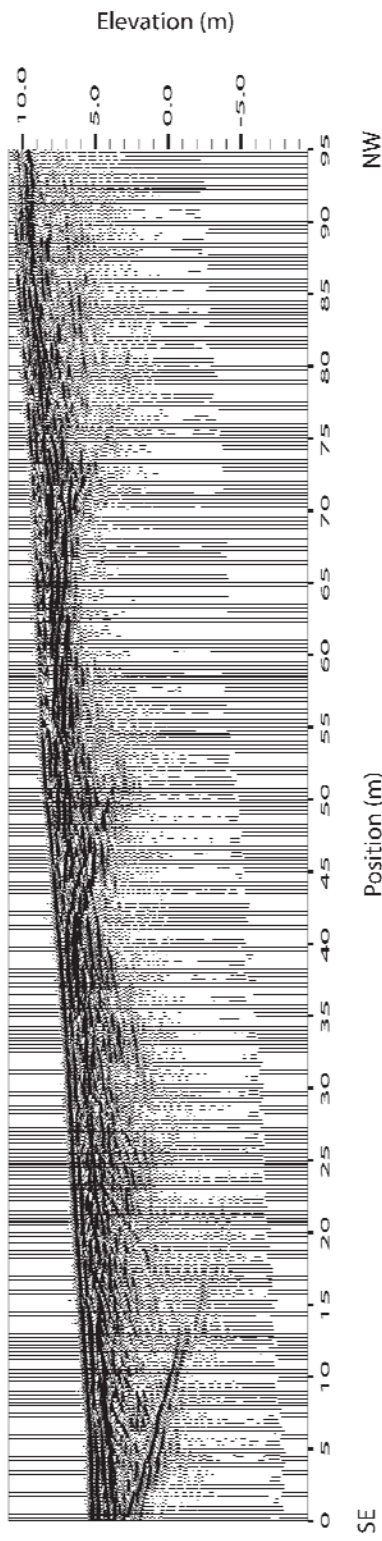


Figure A12 - a) GPR transect T8. Elevation is relative to the water level of East Glacier Lake (3,282m amsl). Depths below ground level are based on an average radar velocity of 0.06 m/ns. b) Interpreted GPR transect T8. Bedrock fractures (F5, F6, and F7) centered at approximately 6, 46, and 73m respectively are shown in red.

a)



b)

